

Simulation Study of Beam-Induced Background at the SuperKEKB Interaction Region

Clement Ng
Department of Physics, The University of Tokyo

February 8, 2010

Abstract

The SuperKEKB B factory in Ibaraki, Japan, will mark a new era in high luminosity accelerator experiments upon its proposed completion in 2013. The upgrade to the current KEKB accelerator will probe the physics of rare flavour decays uniquely accessible through its design luminosity of $8 \times 10^{35} \text{cm}^{-2} \text{s}^{-1}$ and clean e^+e^- environment.

With increases of luminosity however come issues of beam-induced backgrounds, which if not contained will inhibit the upgraded Belle II detector in its goal of precisely measuring these decays. In the time during SuperKEKB's development two design proposals for achieving high luminosity have been seen, one increasing the beam current and the other decreasing the beam size, with different implications for beam background levels in the interaction region.

In this thesis we examine the impact of synchrotron radiation backgrounds from a high-current accelerator design, through simulations accurately modelling backscattering within the IR beampipe. We also present the progress towards simulating radiative Bhabha backgrounds, which will scale with increased luminosity, for the recent nano-beam accelerator design chosen for use at SuperKEKB.

Acknowledgements

I am deeply indebted to Professor Hiroaki Aihara for offering the chance to join this project which has been a long standing dream of mine, and continuing to prove an immense inspiration to me with his insight into the wider picture. I am grateful to Masako Iwasaki for leading me through much new territory and always displaying a fortitude of experience in this field. I thank all of the talented members in this lab, Toshinori Abe, Hidekazu Kakuno, Masashi Yokoyama, Yu Nakahama, Hiroyuki Nakayama, Hironao Miyatake, Hiroki Fujimori, Sogo Mineo and Shinya Sugihara for helping me with so many customs and so many new experiences I cannot begin to list them.

On that point, I am deeply grateful to everyone I have met in this city who make research and life the most incredibly inspiring experience of all.

Most of all I thank my family back home who I now understand are always there to believe in the future I see in everything.

Contents

1	Introduction	9
1.1	Super B Factories and the Luminosity Frontier	9
1.2	The Relationship between Luminosity and IR Design	11
2	The SuperKEKB IR Upgrade	13
2.1	Beam Optics	13
2.1.1	Linear Beam Optics Theory	13
2.1.1.1	Betatron Oscillation	15
2.1.1.2	Luminosity	16
2.1.2	High-Current Design	19
2.1.3	Nano-Beam Design	19
2.2	The Belle II Detector	20
2.2.1	PXD	20
2.2.2	SVD	22
2.2.2.1	CDC	22
2.2.3	PID	22
2.2.4	ECL	22
2.2.5	KLM	22
2.3	IR Structure	23
2.3.1	IP Chamber and IR Beampipe	23
2.3.2	IR Assembly, HOM Heating and Vibrations	25
3	Backgrounds at the SuperKEKB IR	27
3.1	Synchrotron Radiation	27
3.1.1	SR Processes	27
3.1.2	Problems Seen at Belle	28
3.1.3	Considerations for SuperKEKB	28
3.1.3.1	Direct SR	28

3.1.3.2	Backscatter SR	31
3.2	Radiative Bhabha Scattering	33
3.2.1	Radiative Bhabha Processes	33
3.2.2	Problems Seen at Belle	34
3.2.2.1	ECL Background	34
3.2.2.2	KLM Background	35
3.2.3	Considerations at SuperKEKB	37
3.3	Other Backgrounds	37
3.3.1	Beam-Gas Scattering	37
3.3.2	Touschek	38
4	Synchrotron Radiation Background Simulation	39
4.1	Overview	39
4.2	SR Event Generation	39
4.2.1	<i>SAD</i> Beam Optics Simulator	39
4.2.2	<i>LCBDS</i> Beamline Simulator	40
4.3	Beampipe Scattering Simulation	41
4.3.1	Beampipe Model	42
4.3.1.1	IP Chamber	42
4.3.1.2	Outer IR Beampipe	42
4.3.2	Limitations of two-stage simulation	47
4.4	PXD Occupancy	48
4.5	Simulation Analysis	48
4.5.1	Total Energy Deposits from SR	48
4.5.1.1	Study of Previous Optics from 2008	48
4.5.1.2	2009 Optics (1012a)	54
4.5.2	Backscatter SR Analysis	57
4.5.2.1	Track Selection	57
4.5.2.2	HER	57
4.5.2.3	LER	58
4.5.2.4	Aluminium HER Downstream Beampipe	59
5	Radiative Bhabha Background Simulation	61
5.1	Overview	61
5.2	Radiative Bhabha Event Generation	61
5.2.1	<i>BHLUMI</i> Bhabha Simulator	61
5.3	Beamline and Detector Modelling	62
5.3.1	Beamline Structure	62

5.3.2	Belle II Detector	62
5.3.3	Event Filter	64
5.4	Simulation Results	65
6	Further Work and Propects	67
7	Conclusion	68
8	Appendix	69
8.1	Flavour Properties of Kaluza-Klein States	69
8.1.1	Bulk Fermions in Warped Extra Dimensions	70
8.1.2	Kaluza-Klein Graviton Exchange	71

List of Figures

2.1.1	Layout of the accelerator upgrade at SuperKEKB	14
2.1.2	Expected integrated luminosity at SuperKEKB	18
2.1.3	Layout of the magnets in the IR for KEKB/SuperKEKB High Current (top) and SuperKEKB Nano-beam (bottom)	21
2.1.4	Crossing schemes for Head-on (left) and Nano-beam (right) IP	21
2.3.1	Diagram of the IP chamber (centre) connected to the heavy-metal shielded and outer IR beampipes. Distances are given in mm	23
2.3.2	Photo of the current KEKB IP Chamber	24
2.3.3	IR beampipes (yellow) in relation to the Belle II detector	24
2.3.4	Position of magnets in the IR	25
2.3.5	Possible quick-disconnect system for IR assembly	26
3.1.1	Performance of the SVD 1.0 during summer 1999	29
3.1.2	Comparison of SVD energy spectra with steering magnet limits and modifications to the IR beam chamber	29
3.1.3	Axis alignments for LER, HER and Belle solenoids in KEB and SuperKEKB (nano-beam)	30
3.1.4	Displacements in Δx and Δy for the nano-beam HER path inside the combined solenoid and anti-solenoid field B_z	31
3.1.5	IR layout of quadropole magnets in the high-current design (units of m, vertical axis highly scaled)	32
3.2.1	Feynman diagrams for t and s channel Bhabha scattering	34
3.2.2	Radiative Bhabha scattering in the current KEKB IR	35
3.2.3	Radiative Bhabha background in the ECL at Belle from the cur- rent data (left) and simulations after heavy metal shielding (right)	36
3.2.4	Neutron scattering to the KLM from radiative gammas in the KEKB IR chamber	36
3.2.5	Background hit rate (Hz/cm^2) in the Belle KLM endcap before (left) and after (right) installation of polyethylene shield	37

4.2.1	Example of a positron track in a beamline structure created in <i>LCBDS</i>	41
4.2.2	SR emitted from LER beam passing through quadrupole magnets in the IR (IP chamber geometry included)	41
4.3.1	Diagram of the IP chamber model	42
4.3.2	Diagram of the LER downstream side of the IR beampipe; LER pipe is top, HER bottom	43
4.3.3	Diagram of the HER downstream side of the IR beampipe; HER pipe is top, LER bottom	44
4.3.4	LER downstream model in <i>LCBDS</i>	45
4.3.5	HER downstream model in <i>LCBDS</i>	45
4.3.6	Solid visualisation of the LER downstream beampipe (with approximated flanges attached)	46
4.3.7	View of SR colliding with the LER downstream beampipe to produce secondary particles; red tracks are electrons	47
4.4.1	PXD energy deposit simulation for 30 mrad incident photons inside a Be/Au IP chamber (bottom axis is photon energy in keV)	48
4.5.1	2008 Optics SR energy deposit from the LER in the full downstream pipe. For all plots values scaled to one beam bunch. IP is at 0	49
4.5.2	2008 Optics SR energy deposit from the LER near the IP	50
4.5.3	2008 Optics SR energy deposit from the HER in the full downstream pipe	51
4.5.4	2008 Optics SR energy deposit from the HER near the IP; note that hits in the chamber region are exaggerated due to the absence of solenoid field	52
4.5.5	2008 Optics photon energy deposits from the HER around the IP chamber. The equivalent of 200 hits per beam bunch are seen close to the IP (colours represent SR origin; see section 4.5.2)	53
4.5.6	2008 Optics SR deposit summary for the LER downstream IR	53
4.5.7	2008 Optics SR deposit summary for the HER downstream IR	54
4.5.8	Comparison of SR deposits in HER downstream for 2008 (top) and 2009 (bottom) optics, with cut $E_{SR} < 20$ keV. The number of hits is reduced to 1/3 in the new optics	55
4.5.9	Comparison of HER SR energy distribution and SR production origin for 2008 (top) and 2009 (bottom) optics	56
4.5.10	Backscattered SR near the IP from the HER	58
4.5.11	Backscattered SR near the IP from the LER	59
4.5.12	Backscattered SR near the IP from the HER with an aluminium beampipe	60

5.3.1	Diagram of the Belle II detector (IP chamber is for the high-current design)	63
5.3.2	Model in <i>LCBDS</i> of the HER beamline and Belle II detector . . .	64
5.3.3	Run in the LER beampipe showing beampipe hits without an angle-cut	65
5.4.1	Visualisation of Bhabha events in LER beamline	66
5.4.2	Visualisation of Bhabha events in HER beamline	66
8.1.1	$\sin(2\phi_1)_{\phi K_S}$ distribution in the KK gluon mass for decay amplitude phases (bottom to top) $\omega = \frac{\pi}{3}, \frac{\pi}{4}, \frac{\pi}{6}, \frac{\pi}{10}$. The red horizontal band is the world average value for the SM $b \rightarrow c\bar{c}s$ tree level process $B_d \rightarrow J/\psi K_S^0$, $\sin(2\phi_1)_{\psi K_S^0}$	71
8.1.2	$\langle P_3 \rangle$ as a function of scaled momentum transfer s for different graviton scenarios; $M_H = 1$ (red), 1.5, 2 ... TeV for the ADD model (left) and first-mode graviton masses 600 (red), 700, ... GeV for the Randall-Sundrum (right) models	72

List of Tables

1.1.1 Summary of sensitivities for Belle (2003 luminosity; current is 1ab^{-1}), SuperKEKB and LHCb	10
2.1.1 Design beam parameters for KEKB and SuperKEKB	18

Chapter 1

Introduction

1.1 Super B Factories and the Luminosity Frontier

The high energy physics community has reached a crossroad in respect to the ability to independently run and finance the traditional mode of frontier experiments, particle colliders. Since the last major accelerator LHC at Cern, the dividends for new accelerator and upgrade projects have faced closer scrutiny as to how they should weigh up against the rising upfront and ongoing costs of delving into open-ended theoretical territory. In face of the question “What is left to pursue in accelerator experiments when the energy frontier belongs to the LHC?” one of the immediate answers to many is, explore the physics bound by rare decays through pushing the luminosity frontier.

The SuperKEKB accelerator and Belle II detector upgrades at KEK are designed to increase the luminosity, or the rate of collision events per area, of the B factory experiment to breakthrough levels of $8 \times 10^{35} \text{cm}^{-2} \text{s}^{-1}$, and provide a much-anticipated window into flavour physics in the Higgs sector and extensions to the Standard Model. As with the current KEKB collider, SuperKEKB will collide electron and positrons at the $\Upsilon(4S)$ resonance of 10.58 GeV which immediately decay to $B\bar{B}$ meson pairs. While other concurrent accelerator experiments will attempt to probe new physics through higher collision energies, highly-suppressed flavour-mixing channels and new off-mass shell heavy virtual particles offer a more successful chance of detection through the cleaner environments of B factories like SuperKEKB and the proposed SuperB at INFN, Italy, with the aide of better particle identification and large statistics. [1]

Flavour physics can offer hints to new physics in two areas. In flavour changing neutral currents (FCNC), neutral meson-antimeson mixing and CP violation are limited to loop level in the Standard Model and so highly-suppressed. Any observed signals in these channels then point to the possibility of new physics virtual contributions. Similarly, quark flavour violation is suppressed in the

Observable	Belle 2003	SuperKEKB		LHCb
	(0.14ab ⁻¹)	(5 ab ⁻¹)	(50 ab ⁻¹)	(0.002ab ⁻¹)
$\Delta\mathcal{S}_{\phi K_S^0}$	0.51	0.079	0.031	0.2 [168]
$\Delta\mathcal{S}_{K^+K^-K_S^0}$	$^{+0.32}_{-0.26}$	0.056	0.026	
$\Delta\mathcal{S}_{\eta' K_S^0}$	0.27	0.049	0.024	×
$\Delta\mathcal{S}_{K_S^0 K_S^0 K_S^0}$	NA	0.14	0.04	×
$\Delta\mathcal{S}_{\pi^0 K_S^0}$	NA	0.10	0.03	×
$\sin 2\chi (B_s \rightarrow J/\psi\phi)$	×	×	×	0.058
$\mathcal{S}_{K^*0\gamma}$	NA	0.14	0.04	×
$\mathcal{B}(B \rightarrow X_s\gamma)$	26% (5.8 fb ⁻¹)	5%	5%	×
$A_{CP}(B \rightarrow X_s\gamma)$	0.064	0.011	5×10^{-3}	×
C_9 from $\overline{A}_{\text{FB}}(B \rightarrow K^*\ell^+\ell^-)$	NA	32%	10%	
C_{10} from $\overline{A}_{\text{FB}}(B \rightarrow K^*\ell^+\ell^-)$	NA	44%	14%	
$\mathcal{B}(B_s \rightarrow \mu^+\mu^-)$	×	×	×	4σ (3 years) [170]
$\mathcal{B}(B^+ \rightarrow K^+\nu\nu)$	NA		5.1σ	×
$\mathcal{B}(B^+ \rightarrow D\tau\nu)$	NA	12.7σ	40.3σ	×
$\mathcal{B}(B^0 \rightarrow D\tau\nu)$	NA	3.5σ	11.0σ	×
$\sin 2\phi_1$	0.06	0.019	0.014	0.022
ϕ_2 ($\pi\pi$ isospin)	NA	3.9°	1.2°	×
ϕ_2 ($\rho\pi$)	NA	2.9°	0.9°	×
ϕ_3 ($DK^{(*)}$)	20°	4°	1.2°	8°
ϕ_3 ($B_s \rightarrow KK$)	×	×	×	5°
ϕ_3 ($B_s \rightarrow D_sK$)	×	×	×	14°
$ V_{ub} $ (inclusive)	16%	5.8%	4.4%	×
$\mathcal{B}(\tau \rightarrow \mu\gamma)$	$< 3.1 \times 10^{-7}$	$< 1.8 \times 10^{-8}$		
$\mathcal{B}(\tau \rightarrow \mu(e)\eta)$	$< 3.4(6.9) \times 10^{-7}$	$< 5 \times 10^{-9}$		
$\mathcal{B}(\tau \rightarrow \ell\ell)$	$< 1.4\text{-}3.1 \times 10^{-7}$	$< 5 \times 10^{-9}$		

Table 1.1.1: Summary of sensitivities for Belle (2003 luminosity; current is 1ab^{-1}), SuperKEKB and LHCb

Standard Model's small quark mixing angles, allowing for the observation of first-order new physics couplings. *The new physics flavour problem* is a term used to describe the discrepancy between the $O(1)$ TeV scale for new physics suggested by solutions to the Hierarchy Problem and the $O(10^3)$ TeV scale associated with unsuppressed new physics FCNC processes. The inclusion of FCNC suppression in various new models each present distinctive flavour structures which are identifiable at B factories. Present measurements in these sectors largely agree with the Standard Model to $O(10\%)$, so any presence of new physics will only be observed by high-precision experiments, awarding upgrades in luminosity at the B factories a unique opportunity to test these models first.

An often reviewed prospect for new physics searches at Belle II is in SUSY found for example in [1]. Another new physics model that becomes observable at Super B Factories is flavour violation in extra dimension models - an overview of these theories is provided in Appendix 8.1.

1.2 The Relationship between Luminosity and IR Design

Increased luminosity presents many challenges to the interaction region (IR) of SuperKEKB where the e^- High Energy Ring (HER) and e^+ Low Energy Ring (LER) collide and the design of the Belle II detector. A variety of beam-induced background particles expected to increase with the higher luminosity must be studied in full to prevent contamination of detector components and overheating in beam chambers and masks. In the past, failure to properly measure the levels of beam backgrounds at Belle have resulted in forced replacement and redesign of damaged components,[2] and already we are seeing how critical the control of backgrounds has proven to the progress of the SuperKEKB and Belle II designs. Many options for achieving the upgrade goals have been considered and the task of evaluating their impact on the IR is immense, requiring the collaboration of many people from accelerator and detector teams.

Three main sources of background expected to be of concern in the IR are: synchrotron radiation (SR), resulting from on-axis upstream and off-axis downstream beam passage through quadrupole magnetic fields; radiative Bhabha scattering, e^+e^- scattering accompanied by bremsstrahlung radiation at the IP; beam-gas scattering, where the beam scatters and bends in the vicinity of residual gas nuclei; and Touschek scattering, where high densities of electrons within beam bunches elastically scatter off each other.. This thesis will include a study of synchrotron radiation from the “High-current” optics design recently made obsolete at SuperKEKB, and radiative Bhabha scattering from the currently in progress “Nano-beam” optics design. The continued study of IR backgrounds at SuperKEKB will prove crucial to the final structure of many beamline components.

The current KEKB accelerator operates at the world’s highest luminosity of $2.11 \times 10^{34} \text{cm}^{-2}\text{s}^{-1}$, and has accumulated an integrated luminosity of 1000fb^{-1} . This performance originates from its finite crossing-angle, as opposed to head-on collision used in PEP-II at SLAC, which was chosen for its simple implementation, containment of synchrotron background and elimination of parasitic collision beam-beam effects. [4] The results heralded a new standard for future colliders and was marked by some KEKB scientists as a important outcome of the competition between the two B factories. Now, a new optics scheme that again foregoes small crossing-angles for the ability to better focus overlapping regions of the e^+e^- beam - called the nano-beam design - has proved to be the best path towards increasing luminosity beyond another magnitude at SuperKEKB. The fact that the the nano-beam scheme was first promoted by the SuperB planning group for use in their high luminosity B factory in Italy is a telling sign of the nature of high energy physics experiments today. The impact of increasing cuts to government funding and countries pulling out of high-profile experiments cannot be well known in view of the potential loss of technical development, and the international scene has been forced to be more integrated and open than ever in order to stay on top of the changing landscape.

Two experiments may be equal to more than the sum of their luminosities as an increased focus on international feedback can sway the direction of collider technologies tomorrow.

Chapter 2

The SuperKEKB IR Upgrade

In this chapter we explain the interplay of design choices in the IR ecosystem and discuss the scope in which beam backgrounds coinhabit the landscape at SuperKEKB.

2.1 Beam Optics

2.1.1 Linear Beam Optics Theory

The fundamental characteristics of charged particle beam transport is described in the language of linear beam optics. SuperKEKB like KEKB before it is a circular collider, where pre-accelerated electron and positron beams are injected in opposite directions into a large circular-like tunnel known as a storage ring. Over the lifetime of each beam the particle paths are steered into one another at the interaction point (IP) with high-frequencies in order to offset the small cross-sections that govern the probability of a production event. To maximise the lifetime of the beam, the trajectories must be precisely steered and focused as they circulate in the ~3 km long storage ring.

A number of beam parameters that will ultimately determine the luminosity of the collider emerge in linear beam optics, which we briefly describe here. The charged electron and positron beams are fundamentally steered through magnetic field sources at various points in the ring, as per the Lorentz force

$$\mathbf{F} = e(\mathbf{E} + \mathbf{v} \times \mathbf{B}) = \dot{\mathbf{p}} \quad (2.1.1)$$

Adopting the coordinates where z is the longitudinal path of the beam and x and y are transverse horizontal and vertical, we can match the centrifugal force

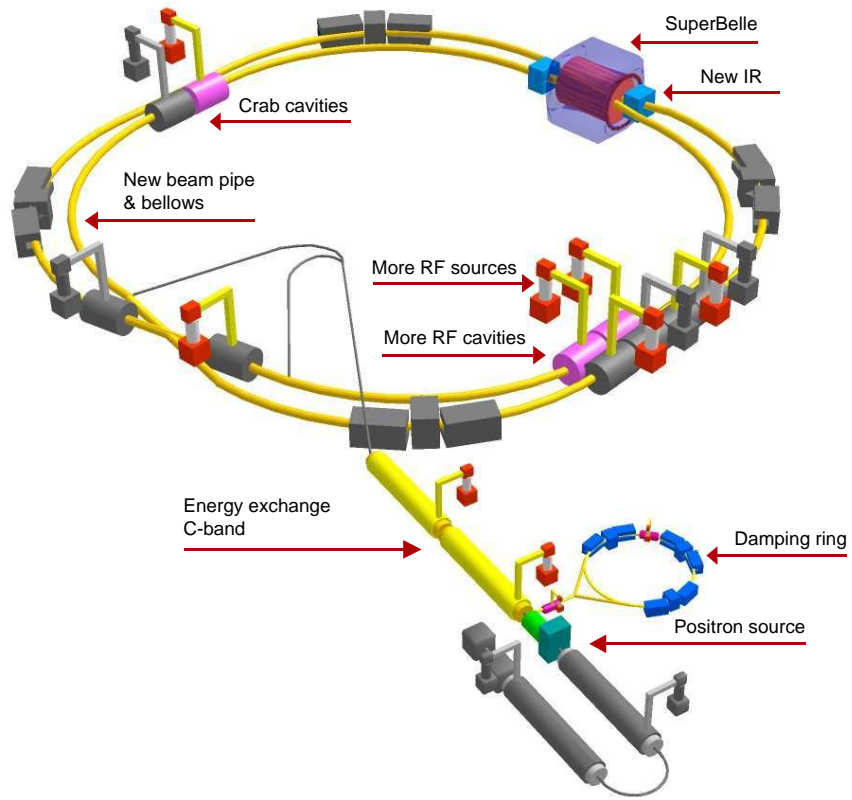


Figure 2.1.1: Layout of the accelerator upgrade at SuperKEKB

$F_r = mv_z^2/R$ of a particle moving in a horizontal curvature of radius R with the Lorentz force $F_x = -ev_z B_y$ to give the relation

$$\frac{1}{R(x, y, z)} = \frac{e}{p} B_y(x, y, z) \quad (2.1.2)$$

Because the transverse dimension of the beam are small compared to the radius of curvature, the magnetic field can be expanded around its nominal trajectory:

$$B_y(x) = B_{y0} + \frac{dB_y}{dx} + \frac{1}{2!} \frac{d^2 B_y}{dx^2} x^2 + \frac{1}{3!} \frac{d^3 B_y}{dx^3} x^3 + \dots \quad (2.1.3)$$

and multiplied by $\frac{e}{p}$ to get

$$\begin{aligned} \frac{e}{p} B_y(x) &= \frac{e}{p} B_{y0} + \frac{e}{p} \frac{dB_y}{dx} + \frac{1}{2!} \frac{e}{p} \frac{d^2 B_y}{dx^2} x^2 + \frac{1}{3!} \frac{e}{p} \frac{d^3 B_y}{dx^3} x^3 + \dots \\ &= \frac{1}{R} + kx + \frac{1}{2!} mx^2 + \frac{1}{3!} ox^3 + \dots \end{aligned}$$

These terms can be interpreted as multipole magnetic field components - dipole, quadropole, sextupole, octupole and so on - with strengths given by their constant coefficients. Vertical trajectories can be similarly related to an expansion in $B_x(y)$. Trajectories affected by fields with orders up to 1 only (i.e. dipole and quadropole) are characterised in linear beam optics theory. The principle effects of these two components are *beam steering* in dipole fields and *beam focusing* in quadropole fields. Higher-order multipole fields will also be taken into consideration when making small corrections to beam-energy dependent effects. [10]

By considering relativistic particles so that the effect of the magnetic field on longitudinal velocity is negligible and assuming small deviations in momentum $\Delta p \ll p$, the basic linear equations of motion relating to horizontal steering and focusing along the longitudinal path z are shown to simplify to: [10]

$$\begin{aligned} x''(z) + \left(\frac{1}{R^2(z)} - k(z) \right) x(z) &= \frac{1}{R(z)} \frac{\Delta p}{p} \\ y''(z) + k(z)y(z) &= 0 \end{aligned} \quad (2.1.4)$$

where the sign for the quadropole strength k is chosen to be positive for horizontal focusing. It is important to note that quadropole fields will only focus the beam in one transverse plane, while simultaneously defocusing the beam in the perpendicular one. Hence accelerators employ both horizontal and vertical focusing quadropole magnets in an alternating layout.

2.1.1.1 Betatron Oscillation

In accelerators, we are interested in describing the overall properties of multiple particles travelling together in the beam. Hill's differential equation of motion

describes the transverse or *betatron* oscillations $x(z)$ in an orbit and formed by assuming that $\frac{1}{R}$ and $\frac{\Delta p}{p}$ in 2.1.4 are zero :

$$x''(z) - k(z)x(z) = 0 \quad (2.1.5)$$

The general solution is found by introducing method of variation of integration parameters as per the harmonic oscillator equation [11]

$$x(z) = \sqrt{\varepsilon} \sqrt{\beta(z)} \cos(\psi(z) - \psi_0) \quad (2.1.6)$$

where ε and ψ_0 are intergration constants. The phase function becomes

$$\psi(z) = \int_0^z \frac{d\bar{z}}{\beta(\bar{z})} + \psi_0 \quad (2.1.7)$$

The amplitude $\pm\sqrt{\varepsilon\beta(z)}$ of the betatron oscillations describe a *beam envelope* marking out the range of possible individual trajectories for a given particle. $\beta(z)$ is known as the beta function and is dependent on the focusing structure along the beam transport system. ε is called the emittance and is a constant of the particle orbit. Multiple particles which are injected into the storage ring in bunches will stochastically inherit slightly differing energies due to synchrotron radiation emission, so we assume the equilibrium transverse particle distribution is gaussian with beam size $\sigma(z)$ and define the nominal emittance by relating $\sigma(z) = \sqrt{\varepsilon\beta(z)}$. Good focusing in an accelerator will always require betatron oscillation to be carefully matched with the quadropole magnet field strengths and layout.

2.1.1.2 Luminosity

The luminosity L directly effects the production rate of $\Upsilon(4S)$ (which will decay to $B\bar{B}$ pairs $> 96\%$ of the time) through the relation $\dot{N}_\Upsilon = \sigma_\Upsilon L$, where σ_Υ is the interaction cross-section of $\sim 10^{-33}$ cm². Assuming that the beta function and beam size are common to both electron and positron beams at the IP, the luminosity is calculated [10] from

$$L = \frac{N_{e^+} N_{e^-} f}{4\pi\sigma_x\sigma_y} R_L \quad (2.1.8)$$

Here f is the beam bunch collision frequency and N the number of particles in each bunch for the positron and electron beams. R_L is the luminosity reduction factor to describe geometrical reduction due to ‘‘hour-glass’’ collisions that arise outside the IP, affected by a finite crossing angle θ_x and bunch length σ_z :

$$R_L = \frac{a}{\sqrt{\pi}} e^b K_0(b) \quad (2.1.9)$$

where K_0 is the Bessel function and

$$\begin{aligned} a &= \frac{\beta_y}{\sigma_z} \\ b &= \frac{a^2}{2} \left(1 + \left(\frac{\sigma_z}{\sigma_x} \tan \frac{\theta_x}{2} \right)^2 \right) \end{aligned}$$

The frequency f is equal to the RF frequency at KEKB of 508.9 MHz. The number of particles per bunch is given by

$$N = \frac{I}{ef} \quad (2.1.10)$$

where I is the beam current and e the electron charge. It is clear from this that two general methods for increasing luminosity are decreasing the beam size and increasing the beam currents.

L is often expressed in terms of the beam-beam parameter ξ , a quantity related to the shift in phase advance per orbit (betatron tune), by:

$$\begin{aligned} L &= \frac{\gamma_{e^\pm}}{2er_e} \left(1 + \frac{\sigma_y}{\sigma_x} \right) \left(\frac{I_{e^\pm} \cdot \xi_{y,e^\pm}}{\beta_y} \right) \left(\frac{R_L}{R_{\xi_y}} \right) \\ \xi_{x,y,e^\pm} &= \frac{r_e}{2\pi\gamma_{e^\pm}} \frac{N_{e^\mp} \cdot \beta_{x,y}}{\sigma_{x,y}(\sigma_x + \sigma_y)} R_{\xi_{x,y}} \end{aligned}$$

where r_e is the classical electron radius, γ the Lorentz factor (γI assumed to be equal at IP for both e^+ and e^-) and R_ξ the reduction factor for the beam-beam parameter defined in [3].

At SuperKEKB the beam at the IP has a ‘‘flat’’ focus where $\sigma_y \ll \sigma_x$ and ratio of reduction factors $\frac{R_L}{R_{\xi_y}} \approx 0.8$, so that the luminosity is approximately

$$L \approx \frac{\gamma_{e^\pm}}{2er_e} \frac{I_\pm \xi_{y,e^\pm}}{\beta_y} \quad (2.1.11)$$

Attempts to maximise the luminosity through I , ξ_y or β_y each face their own constraints. Large beam currents increase the wall-plug power costs as well as beam-pipe heating through synchrotron emission and higher order modes. The beam-beam parameter has been shown to saturate around ~ 0.14 at high beam currents due to beam-beam interactions which distort the equilibrium gaussian distribution. [3] Decreasing the beta function usually by placing the final-focusing quadrupole magnets as close to the IP as possible presents technological and engineering problems. During SuperKEKB’s conception two main beam optics designs for optimising the luminosity were considered, and are described as follows.

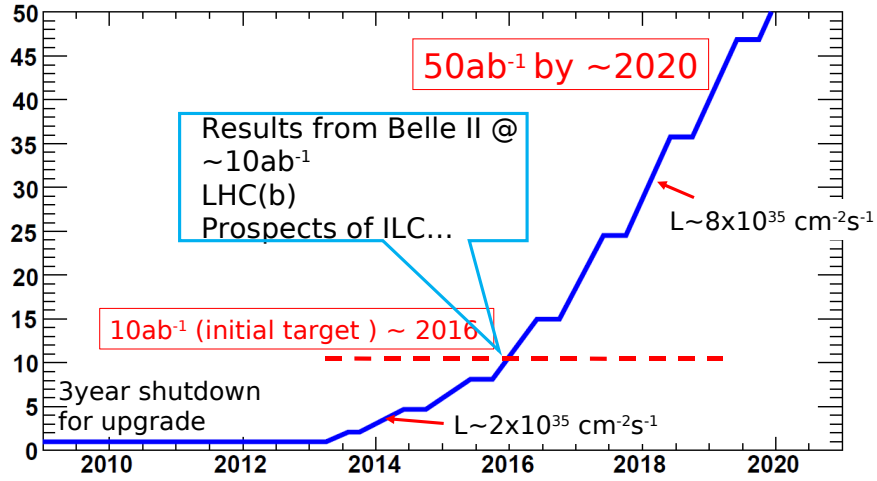


Figure 2.1.2: Expected integrated luminosity at SuperKEKB

Parameter	KEKB		SuperKEKB	
	Design	Achieved	High-current	Nano-beam
LER/HER	10/10	5.9/5.9	3/6	0.27/0.42
β_y [mm]	10/10	5.9/5.9	3/6	0.27/0.42
σ_y [μm]	1.9	1.1	0.85/0.73	0.084/0.072
ξ_y	0.052	0.101/0.096	0.3/0.51	0.088/0.09
I [A]	2.6/1.1	1.62/1.15	9.4/4.1	3.6/2.6
L [$10^{34}\text{cm}^{-2}\text{s}^{-1}$]	1	2.1	53	80

Table 2.1.1: Design beam parameters for KEKB and SuperKEKB

2.1.2 High-Current Design

The SuperKEKB high-current design was the first one studied by the collaboration, motivated by successes in the current KEKB luminosity and a relatively straight-forward method of extending it. In this design beam currents are increased around five times the KEKB values of 1.8A in the positron low energy ring (LER) and 1.45A in the electron high energy ring (HER) to 9.4A and 4.1A respectively. New beam pipe and vacuum components are installed to cope with the current, a new ante-chamber designed to reduce the electron cloud effect and a larger number of RF stations introduced to increase RF power. Implemented on top of the crab cavity scheme newly installed at KEKB, simulations had predicted high beam-beam parameters of 0.3 and 0.51 for the LER and HER, and an IP vertical beta function of 3 mm from the new IR optics design. In total, an increase of around 40 times current luminosities was expected, a target value of $8 \times 10^{34} \text{cm}^{-2} \text{s}^{-1}$.

The crab cavity upgrade, designed to rotate each beam bunch in the horizontal plane by half of the crossing-angle to produce an effective head-on collision, was expected to increase the beam-beam parameter by 2-4 times. After installation at KEKB in 2007 however it was seen that the increase in specific luminosity (luminosity per bunch normalised by bunch current) was only 30%, failing to display the expected linear increase with bunch current. The exact cause to date was not fully uncovered. After additional study proposing a travelling wave scheme to deal with coherent synchrotron light stretching of bunch lengths, a contributor to hour-glass effects, the baseline design luminosity was set at $5 \times 10^{35} \text{cm}^2 \text{s}^{-1}$.

Early IR background studies were also presenting concerns for the large amount of synchrotron light in the HER generated at the final focusing quadrupole magnet, which heat the IP chamber mask and beampipe components. The high-current design is similar to the existing KEKB design in that both electron and positron beams pass through the innermost QCS quadrupole magnets, resulting in bending due to beam translation and rotation offsets with respect to the quadrupole axis and synchrotron emission. (figure 2.1.3) The stronger focusing fields plus increased current resulted in energy deposits which would melt the mask, leading to a redesign in the placement of IR magnets.

In light of the problems emerging in reaching the original target performance, in 2009 the committee decided to drop the high-current design in favour of the nano-beam scheme they had begun to also study in conjunction with the SuperB design team at INFN in Italy.

2.1.3 Nano-Beam Design

The nano-beam design is a recent idea that gained attention for the use in *B*-factories after its proposal at SuperB. Rather than employing drastic changes to beam currents, luminosity is increased by reducing vertical IP beam sizes to nanometer scale and taking advantage of a large crossing-angle mechanism.

In small-angle and head-on crossing schemes the effective longitudinal overlap d of the crossing beams is given by the bunch length σ_z and be much smaller than β_y to avoid hour-glass effects. In a scheme with large crossing-angle ϕ and narrow beam sizes however this overlap is effectively reduced to $d = \frac{\sigma_x}{\phi}$, relaxing the constraint on β_y and the bunch length (figure 2.1.4). Longer bunch length alleviates problems of coherent synchrotron radiation and reduces higher-order mode heating. The modest increase in beam current, combined with the reduction in LER/HER beam energy asymmetry design from 3.5/8 to 4/7 GeV will result in energy run requirements comparable to KEKB. The large-angle concept as well as the “crab-waist” adopted by SuperB, where strong sextupoles magnets are arranged π and $\frac{\pi}{2}$ out of phase of the x and y axes respectively on either side of the IP in order to suppress vertical betatron and synchrotron resonances, were successfully demonstrated at the DAΦNE Φ -factory at INFN in 2007. [12]

The larger crossing-angle offers room for installing separate final-focus QCS magnets in each ring, allowing them to align with the beam axes. This not only facilitates the precise focusing required for the small beam sizes, but also minimises synchrotron radiation from upstream and downstream of the IP, rendering this background extremely small. Diameters must be shrunk one-sixth of the size of present KEKB magnets to 4-8 cm, and efficient cooling will be essential as current density in the superconductors will rise above 2000A/mm², equivalent to temperatures of over 1000K. Great demand will be placed on their manufacturing precision to achieve field errors of a few 10⁴ with respect to the quadrupole field.

The challenge of successfully implementing the nano-beam design at SuperKEKB will be extremely technical, being a compact and delicate scheme requiring careful study and assembly.

2.2 The Belle II Detector

A detector of suitable fine response is essential for pairing with high-luminosity colliders. Harmonising the requirements of detector background limits with acceptable beam performance makes the discussion between accelerator and detector teams crucial. A bare description of the role each Belle II component plays is given here.

2.2.1 PXD

The Pixel Detector is the inner most layer in Belle II, designed to augment the SVD by enhancing the determination of the B decay vertex. Each pixel is a p -channel FET on a depleted bulk of 50 $\mu\text{m} \times 75 \mu\text{m}$. It consists of two layers each with around 2.7M pixels, that cover a 17 to 150 degree region.

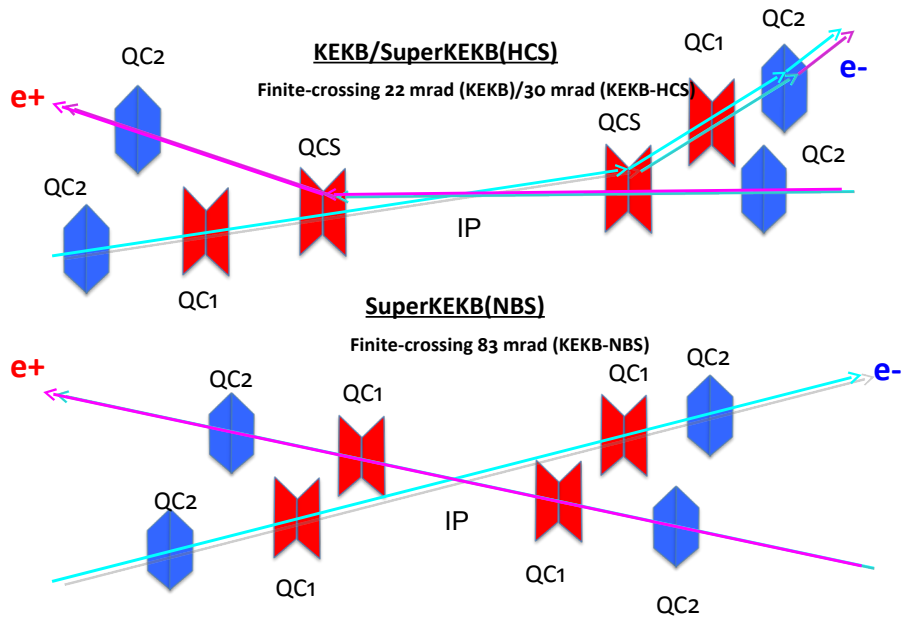


Figure 2.1.3: Layout of the magnets in the IR for KEKB/SuperKEKB High Current (top) and SuperKEKB Nano-beam (bottom)

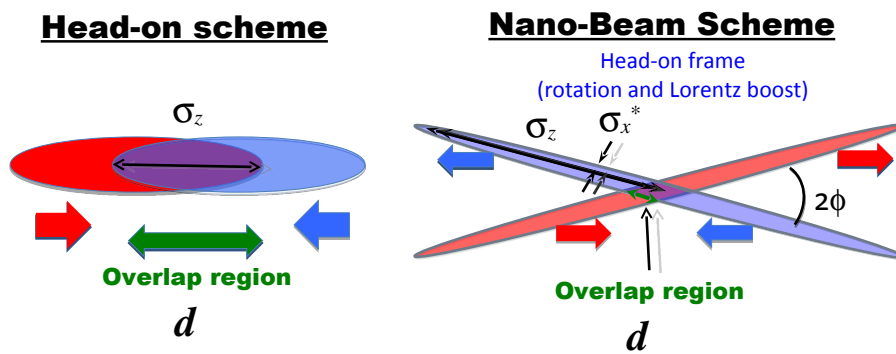


Figure 2.1.4: Crossing schemes for Head-on (left) and Nano-beam (right) IP

2.2.2 SVD

The Silicon Vertex Detector following on from Belle consists of layered-structures of p and n doped Double-Sided Silicon Detectors which obtain two-dimensional position information from electron-hole pair drift created from passing particles. It contains 4 layers that calculate with less precision but wider acceptance than the PXD.

2.2.2.1 CDC

The surrounding Central Drift Chamber is designed to detect momentum of charged particles passing through helium-ethane gas in a 1.5 T magnetic field activated by a superconducting solenoid. Passing particles dislodge drift cell electrons from the gas atoms which then are read by a cage of sensor wires to provide helical information about their motion. From this rate of energy loss as a function of the particle's velocity can be determined, corresponding to a particular momentum and mass combination.

2.2.3 PID

The Particle Identification Device is the biggest change to the new detector, replacing the Cerenkov and Time of Flight counters in Belle. PID will use a time of propagation (TOP) counter, which measure propagation time of Cerenkov photons and a single-dimension position of particles from ring imaging. It provides the clearest determination of K mesons from pions. The design is compact and will be installed in the barrel and endcap.

2.2.4 ECL

The Electromagnetic Calorimetry Layer is the ending point for gamma-rays and electrons, absorbing all of their energy into wedged-shaped calorimeter crystals which produce electromagnetic showers through bremsstrahlung and pair production. Acting also as scintillation detectors, the light emitted from the offspring electrons and positions read through photodiodes reveal the energy of the incident gamma-ray or electron. In the case of an electron this information is then matched with the momentum track left in the CDC.

2.2.5 KLM

The outermost component, the K -Long Muon detector, provides layers of iron plates interspaced with parallel Resistive Plate Chambers that detect ionised discharge of the remaining particles yet to be absorbed. Hadrons will create hadron showers passing through matter and be rapidly absorbed by the iron, whereas muons should penetrate much further. Because muons also leave charged tracks throughout the SVD, CDC and TOF it should be clearly recognisable, and easily

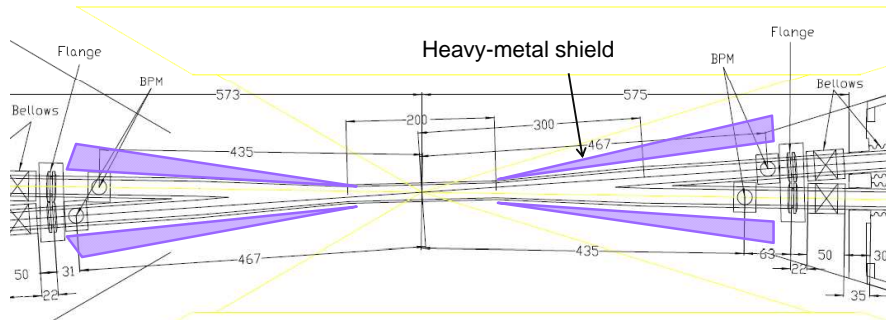


Figure 2.3.1: Diagram of the IP chamber (centre) connected to the heavy-metal shielded and outer IR beampipes. Distances are given in mm

distinguished from the chargeless K -long meson, which would leave identifiable tracks in the KLM only and nothing else.

2.3 IR Structure

2.3.1 IP Chamber and IR Beampipe

At the centre of the IR the LER and HER beampipes meet and collisions are recorded by the surrounding Belle II detector. An IR structure design accommodating the nano-beam scheme is still in the preliminary stage and will be confirmed by the end of 2010, so the parameter values presented here are only tentative.

Around the IP a 20cm straight beryllium chamber with inner radius 10 mm and thickness of around 2mm sits just inside the first layer of the Belle II Pixel Detector (PXD). The choice of beryllium offers weak shielding to low-energy synchrotron photons while almost transparent to all other decay particles, and a small radius allows better calculation of the decay vertex by the PXD. Depending on the result of SR background simulations circular masks may also be installed inside the pipe ends. Attached to both ends of the IP chamber are thick conical titanium shields necessary to prevent background particles from the IR breaking through into the detector.

Joining the IP chamber are V-shaped beampipes extending to the LER and HER upstream and downstream chambers. The beampipe radii are the same as the IP through to the QC1 quadrupole magnets, and widened in steps outside. The beampipe material is copper of approximately 4mm thickness. The ultimate geometry and material of the outer IR beampipes will be made whilst considering the impact of scattered background particles.

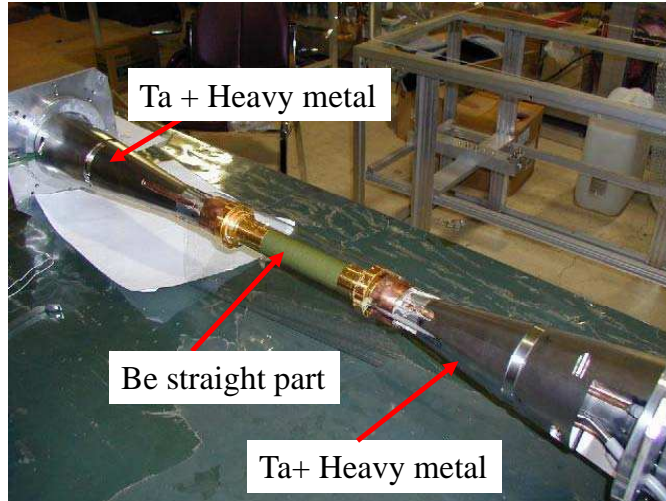


Figure 2.3.2: Photo of the current KEKB IP Chamber

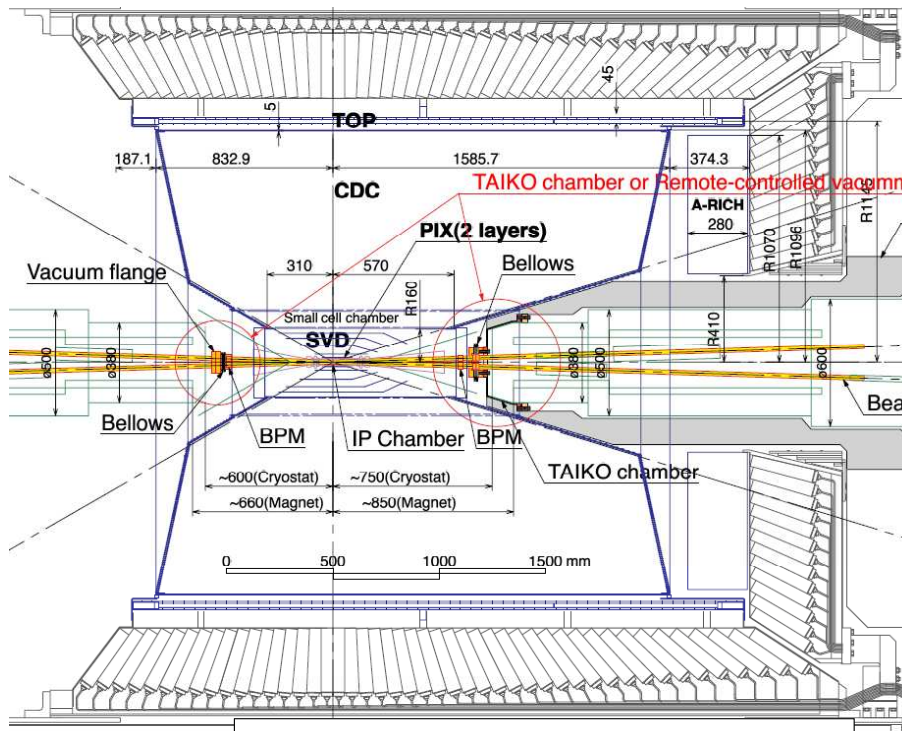


Figure 2.3.3: IR beampipes (yellow) in relation to the Belle II detector

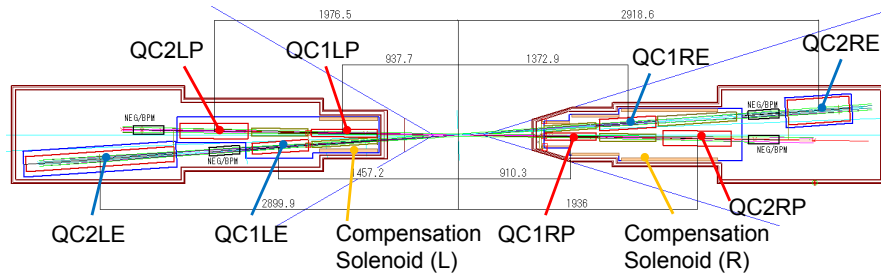


Figure 2.3.4: Position of magnets in the IR

2.3.2 IR Assembly, HOM Heating and Vibrations

The large 83 mrad crossing-angle in the beam optics design is necessitated by space issues in the IR, where required vertical beta functions dictate quadrupole magnets be placed extremely close to the IP. The tightness of the IR configuration presents many engineering issues as to which components must be pre-assembled prior to installation and how to accommodate cooling ducts and electrical cabling. A new method for connecting the massive and tightly integrated components together through remote-controlled vacuum fitting is currently under investigation.

The ultimate shape of the IR chamber must avoid longitudinal trapping of Higher Order Modes (HOM). For this reason the IP chamber radius is set to be smaller than QC1 quadrupole inner radius. The current calculations of HOM heating in the SuperKEKB IP chamber suggests a smaller loss factor than KEKB, however excited transverse modes trapped in the IP chamber produced by deviations of the beam from the pipe center are also being investigated.

In addition, the nano-scale size of the beam at the IP requires that the stability of the support structure be carefully ensured. Vibrations from the natural environment, air conditioning and other sources are presently being studied.

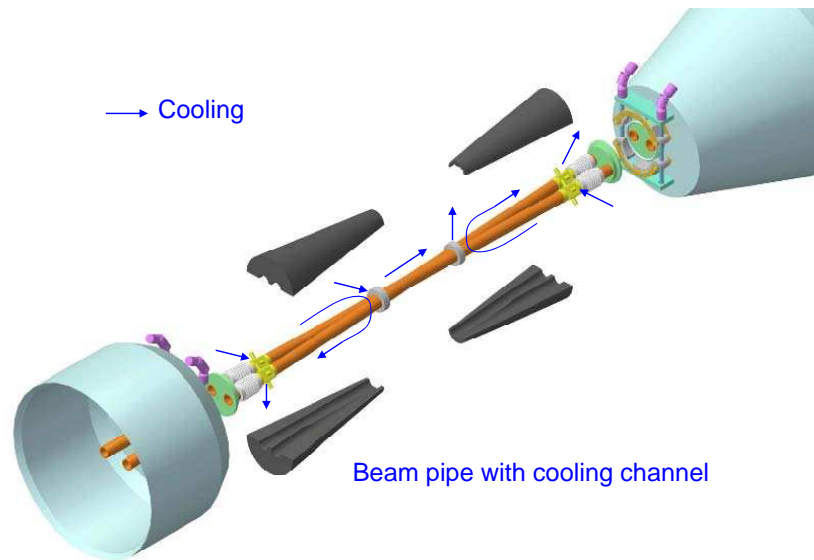


Figure 2.3.5: Possible quick-disconnect system for IR assembly

Chapter 3

Backgrounds at the SuperKEKB IR

3.1 Synchrotron Radiation

3.1.1 SR Processes

Synchrotron radiation (SR) is a phenomenon of photon emission from an accelerating relativistic charged particle. The electric field of a charge particle is moving with constant finite velocity during the motion resulting in a distortion of their field lines that propagates away as energy in the form of electromagnetic radiation. Relativistic Doppler effect and time contraction result in a γ^2 increases in emitted frequencies, and relativistic forward beaming magnifies their intensity in the direction of the moving particle.

In the storage rings, electron and positrons are subject to transverse acceleration from primarily from magnetic steering fields. Assuming that $\gamma = \frac{E_{beam}}{m_e c^2}$ for relativistic beams the emitted SR power and critical energy is given by

$$\begin{aligned} P_s &= \frac{4\pi r_c}{3e} \frac{1}{(m_e c^2)^3} \frac{E_{beam}^4 I}{R} \\ E_c &= \frac{3\hbar c}{2} \frac{1}{(m_e c^2)^3} \frac{E_{beam}^3}{R} \end{aligned} \quad (3.1.1)$$

where R is the bending curvature radius and I is the beam current. [10]

In addition to bending in outer region dipole magnets, off-axis beams with transverse offset d entering the final focus quadrupole magnets will also experience a bending $\frac{1}{R} = \frac{e}{pc} kd$, so depending on the IR optics layout SR can pose a significant detector background. Incident photons of sufficient energy are able to penetrate the beryllium IP chamber and enter the surrounding Belle II Pixel Detector (PXD). In order to keep PXD occupancy levels to less than 1%, the

synchrotron background must be below 50 hits per beam bunch (this is discussed in 4.4). There are two types of SR that can reach the PXD, *direct* SR from the incoming beam passing through upstream steering and quadropole magnets, and *backscatter* SR from the outgoing beam passing through the downstream magnets reflecting off walls of the beam pipe back into the IP.

3.1.2 Problems Seen at Belle

Insufficient consideration of these backgrounds at the beginning of Belle's run led to the damage of the innermost SVD from HER SR in the summer of 1999. The gain readout of the chips dropped suddenly and would later be found to have suffered from a radiation dose over 300 kRad, greater than the limit of 200 kRad. In addition the QCS SR deposits on the IR beampipes caused unexpected heating and deformation, leading to motion of the magnets.

Soft forward SR deposits from 10 keV photons emitted in upstream QC1 quadropole and BC3 steering magnets were deemed to be the cause, resulting in limits placed on steering strength. It was also determined that the SVD and Central Drift Chamber (CDC) were exposed to hard backscattered SR from the HER passing off-axis through the downstream QCS quadropole, impacting 9m further down the beam pipe and scattering 40 keV photons back into the detector. [2] Change of the downstream pipe material from aluminium to copper as well as adding a film of 20 μm gold inside the beryllium IP chamber led a reduction of the backscattered SR to 1/10 of the original levels (figure 3.1.2).

In response to these findings further background SR studies would be conducted at Belle and used to design the new IP chamber during the SVD 2.0 upgrade. Backscatter SR studies in the IR are now considered a crucial phase of any high-luminosity accelerator upgrade.

3.1.3 Considerations for SuperKEKB

We discuss SR issues involved in the high-current design studied in this thesis as well as the nano-beam design to be employed at SuperKEKB.

3.1.3.1 Direct SR

Nano-Beam Design

The separated final-focus design of the new nano-beam scheme allows for the dedicated axis-alignment of quadropole magnets along each of the LER and HER crossing paths. Hence despite the roughly doubled currents in the beam this layout will produce marked reductions in the total amount of produced SR in the IR. In addition to the production from upstream steering magnets which have greater field strength than KEKB's IR, one other consideration that will require study is the a vertical displacement of the beams introduced by a large design offset in horizontal angle to the Belle II superconducting solenoid; 33

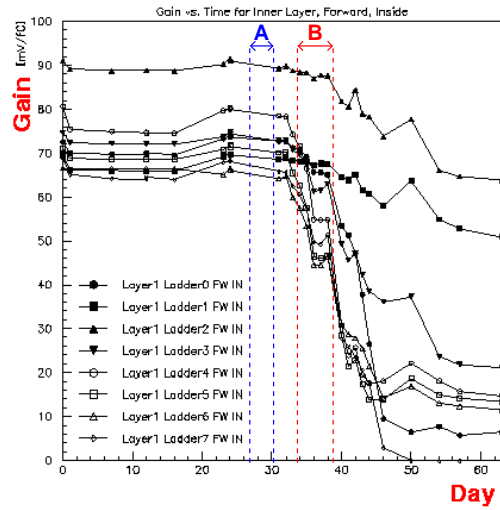


Figure 3.1.1: Performance of the SVD 1.0 during summer 1999

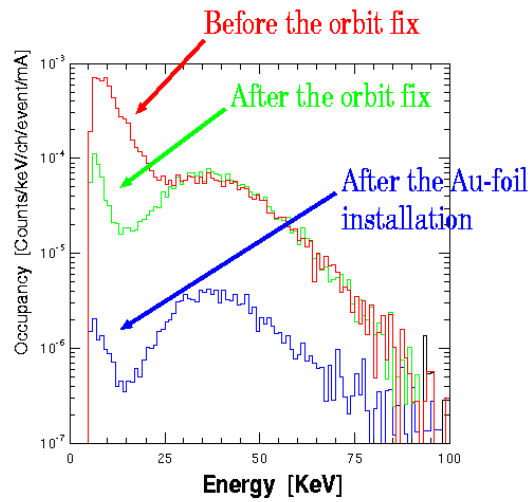


Figure 3.1.2: Comparison of SVD energy spectra with steering magnet limits and modifications to the IR beam chamber

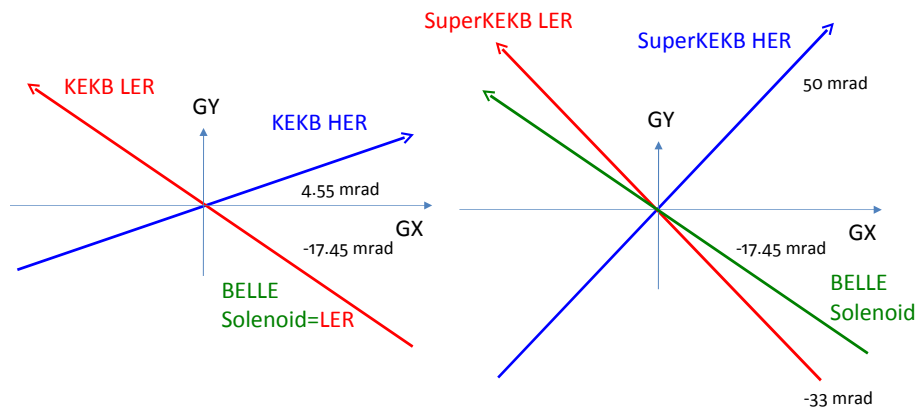


Figure 3.1.3: Axis alignments for LER, HER and Belle solenoids in KEB and SuperKEKB (nano-beam)

4.55 mrad in the LER beamline and 67.45 mrad in the HER (figure 3.1.3). This rotation offset is required in the nano-beam design to facilitate a large bending angle in the HER local chromaticity correction. As a result the beams will feel a net vertical bending when entering at horizontal angles to the solenoid and anti-solenoid longitudinal field, and also a spiral trajectory partly accommodated for by rotation of the quadrupoles along the field.

Depending on the results of the nano-beam simulation appropriate choices of SR masks inside the IP chamber will be made to shield direct SR from the chamber.

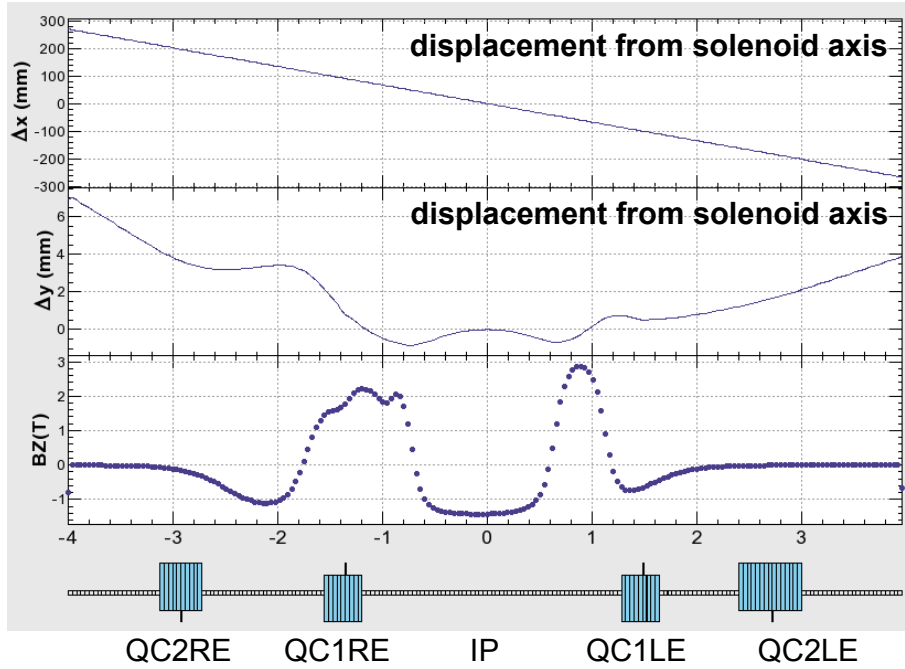


Figure 3.1.4: Displacements in Δx and Δy for the nano-beam HER path inside the combined solenoid and anti-solenoid field B_z

High-Current Design

The high-current design which this thesis presents its simulation study on shares a similar quadrupole layout to KEKB with QCS magnets common to both LER and HER beams, and hence required careful design to alleviate ~ 6 times greater SR power from increases in beam current and high focusing field gradients. While the beam current for the LER of 9.4A is greater than the HER of 4.1A, the E_{beam}^4 term in 3.1.1 dominates and SR power issues will be more severe for the HER. One previous optics design was calculated to deposit over 1kW of SR from the HER to the 4mm wide IP chamber mask that would clearly result in it melting. The last optics design before dropping the high-current scheme lowered this amount to ~ 100 W, ten times the amount at KEKB, but clearly more testing remained to be done for this scheme.

3.1.3.2 Backscatter SR

Three main processes of x-ray emission contribute to the backscatter of SR from the surface of a beam pipe. While in general there will be even larger wattages of secondary electrons from the collisions these are of less concern to the detector as their low-momentum allows the solenoid magnetic field to sweep them away from the IP. The flux and direction of x-ray emission will be dependent on the SR

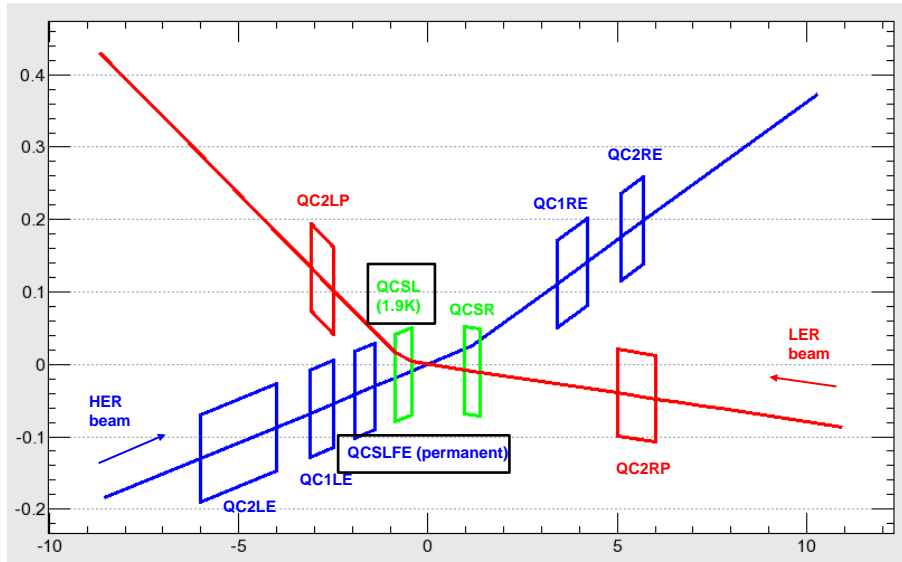


Figure 3.1.5: IR layout of quadrupole magnets in the high-current design (units of m, vertical axis highly scaled)

energy and the atomic properties of the beam pipe material, with cross-sections as follows: [13]

- **Rayleigh Scattering**

$$\frac{d\sigma_R}{d\Omega} = \frac{d\sigma_T}{d\Omega} (F(q, Z))^2 \quad (3.1.2)$$

Here $F(q, Z)$ is the atomic form factor as a function of momentum transfer q and atomic number Z and σ_T is the Thomson cross-section. Backward angles (high momentum transfer) will be larger for low-energy x-rays.

- **Compton scattering**

$$\frac{d\sigma_C}{d\Omega} = \frac{d\sigma_{KN}}{d\Omega} S(q, Z) \quad (3.1.3)$$

σ_{KN} is the Klein-Nishina cross section and $S(q, Z)$ is the incoherent scattering function. Backscattering is large for high-energy x-rays. For $E_\gamma \sim 20$ keV in Copper both Rayleigh and Compton cross-sections are equal.

- **Photoabsorbtion followed by x-ray fluorescence**

The cross-section for photoabsorbtion processes goes as

$$\sigma_P \propto \frac{Z^5}{E^{\frac{7}{2}}} \quad (3.1.4)$$

For incident SR at K edge energies of the material, relaxed emission through x-ray fluorescence can also follow depending on the K-shell properties of the material. L-shell emission is also present for high- Z materials at but at reduced yields, making them effective suppressors of L edge x-rays.

Because the ratio of absorbed to scattered radiation goes as $\sim Z^3$, for energies outside of K edge high- Z materials such as gold offer greater SR absorption and can be chosen to fit the chamber design in the IR.

Nano-Beam Design

Measures to counter backscattered SR in the nano-beam scheme are likely to be minimal as downstream-emitted SR is mitigated through on-axis beams exiting the quadropole magnets. There will be a freedom of choice to cutdown on the complexity and cost of the IR material depending on the severity of incident SR levels.

High-Current Design

The focus of the high-current IR chamber was to provide sufficient clearance for SR fans down to the QC2 quadropole region. As shown in KEKB the backscattering of SR can be reduced by choice of beampipe materials such as an inside $10\mu\text{m}$ gold film to absorb high-energy SR. Bending of the downstream LER beam is slightly greater than the HER leading to wider SR fans although the lower beam energy means the energy spectrum is much lower.

3.2 Radiative Bhabha Scattering

3.2.1 Radiative Bhabha Processes

Bhabha scattering is the interaction of $e^+e^- \rightarrow e^+e^-$ states allowable by annihilation and scattering diagrams in QED with differential cross-section

$$\frac{d\sigma}{d\Omega} = \frac{\alpha^2}{2s} \left(\frac{1 + \cos^4\frac{\theta}{2}}{\sin^4\frac{\theta}{2}} - \frac{2\cos^4\frac{\theta}{2}}{\sin^2\frac{\theta}{2}} + \frac{1}{2}(1 + \cos^2\theta) \right) \quad (3.2.1)$$

where α is the fine structure constant and $\sqrt{s} = (p_1 + p_2) \gg m_e$. It's large well-understood forward cross section makes it useful for measuring the luminosity measurements of the beam.

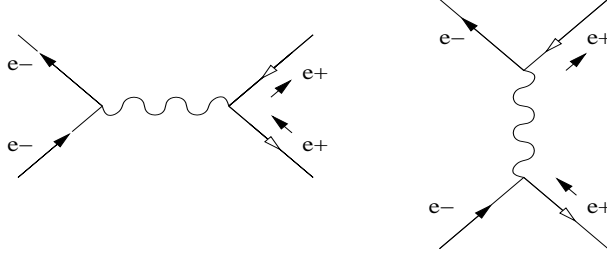


Figure 3.2.1: Feynman diagrams for t and s channel Bhabha scattering

The term “radiative Bhabha scattering” is used for processes taking into account the energy of a final state photon $e^+e^- \rightarrow e^+e^-\gamma$, which in general will always be radiated in any non-zero angle scattering of charged particles. Low-angle scattered Bhabha events fall outside of the detector acceptance range and the photon and off-momentum electron and positrons can scatter in the IR, posing a background for endcap components of the detector. Because radiative Bhabha backgrounds are process dependant they will scale with increases in luminosity rather than beam current.

For low angles the annihilation process dominates, and radiation can occur in either before or after the boson exchange. The scattering angles for outgoing electron/positron and the photon are roughly

$$\theta_\gamma \sim O\left(\frac{1}{\gamma}\right) = \frac{E_{beam}}{m_e}$$

$$\theta_e \sim \frac{1-w}{\gamma} \sim \frac{E_{beam}E_\gamma}{m_e(E_{beam} - E_\gamma)}$$

where $w = \frac{P_{e||}}{P_e} \approx \frac{E_e}{E_{beam}}$.

In the ultrarelativistic limit the differential cross section for outgoing electron/positron and the photon are

$$\frac{d\sigma_e}{dw} = \frac{4\alpha r_e^2}{1-w} \left(1+w^2 - \frac{2}{3}w\right) \left(\ln \frac{s}{m_e^2} \frac{w}{1-w} - \frac{1}{2}\right)$$

$$\frac{d\sigma_\gamma}{dy} = \left(y^2 + \frac{4}{3}(1-y)\right) \left(\ln \frac{s}{m_e^2} \frac{1-y}{y} - \frac{1}{2}\right)$$

where $y = 1-w = \frac{E_\gamma}{E_{beam}}$. In the presence of external fields other QED radiative corrections can also contribute. [13]

3.2.2 Problems Seen at Belle

3.2.2.1 ECL Background

At Belle that a HER downstream luminosity dependent background was observed in Electronic Calorimeter (ECL) readouts, a component in outer region

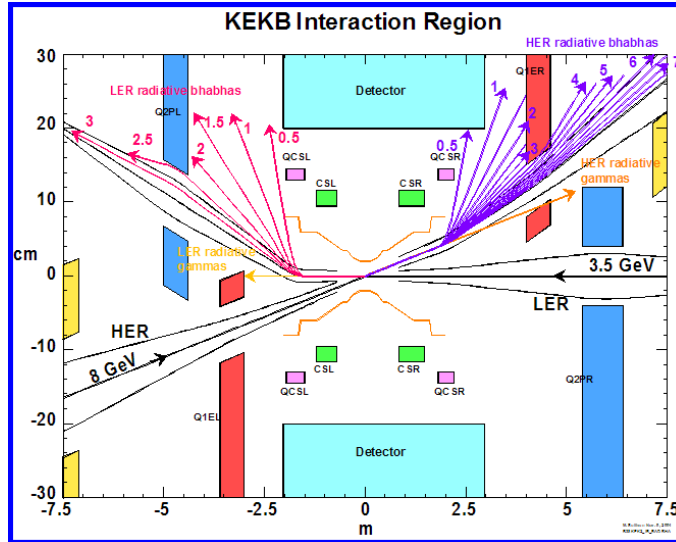


Figure 3.2.2: Radiative Bhabha scattering in the current KEKB IR

of the detector. It is proposed that this is due to off-momentum scattered Bhabha electrons bending inside the downstream QCS magnet and penetrating into the QCSR cryochamber, causing electromagnetic cascade in the material proportional to the energy to reach the ECL. In other detectors such as BaBar at SLAC, radiative Bhabha was a significant background in a zero-crossing angle IR design. [14]

To counter this, simulations suggest that heavy metal shielding incorporated into the QCS magnet should be able to contain this background to $\sim 4\%$.

3.2.2.2 KLM Background

Similarly, luminosity runs demonstrated that scattered Bhabha electrons and positrons which impacted upon downstream beam pipe was a source for scattered neutrons backgrounds into the K-long Muon detector (KLM), the outermost component of the Belle detector. In addition, it is also found that radiative photons hitting the magnets in the HER downstream scatter neutrons in the KLM endcaps.

In 2006 a polyethylene shield placed just outside the endcap was installed which reduced the background by 1/2. Current studies are also investigating how to block apparent neutrons from closer regions such as the QC1 by modifying the geometry of the shield.

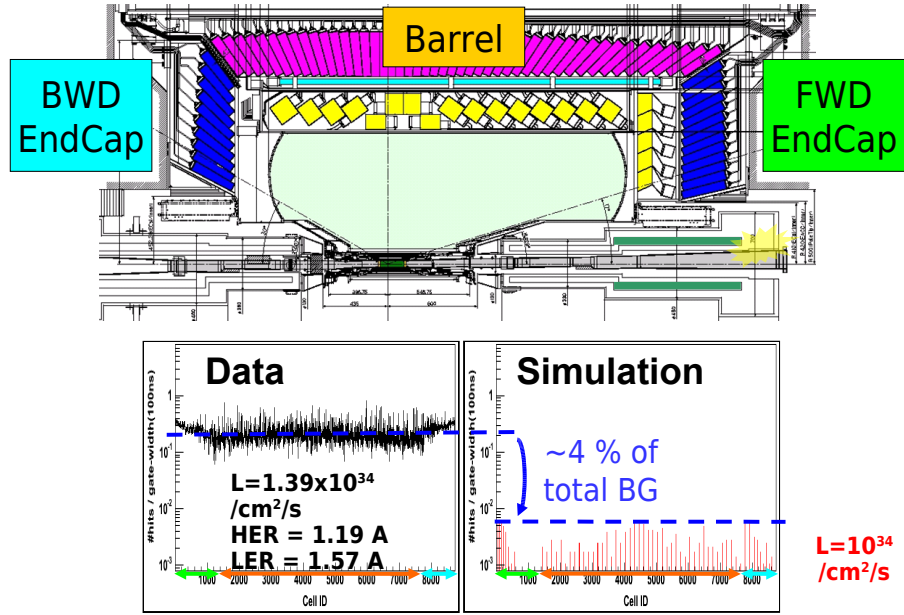


Figure 3.2.3: Radiative Bhabha background in the ECL at Belle from the current data (left) and simulations after heavy metal shielding (right)

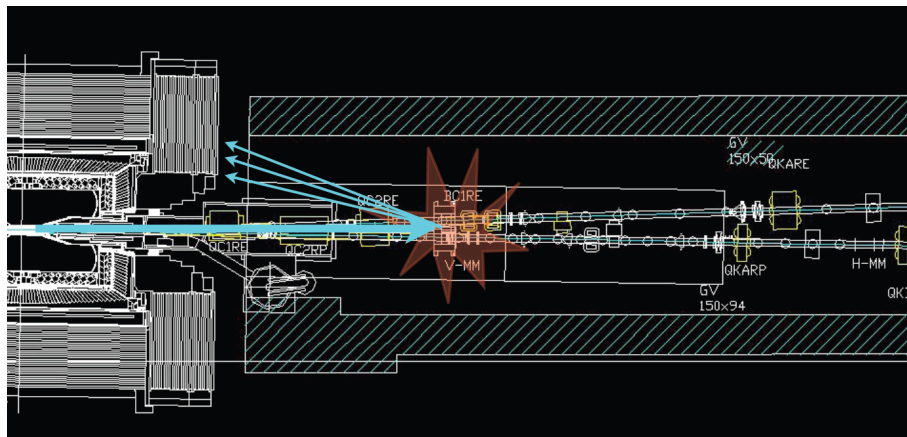


Figure 3.2.4: Neutron scattering to the KLM from radiative gammas in the KEKB IR chamber

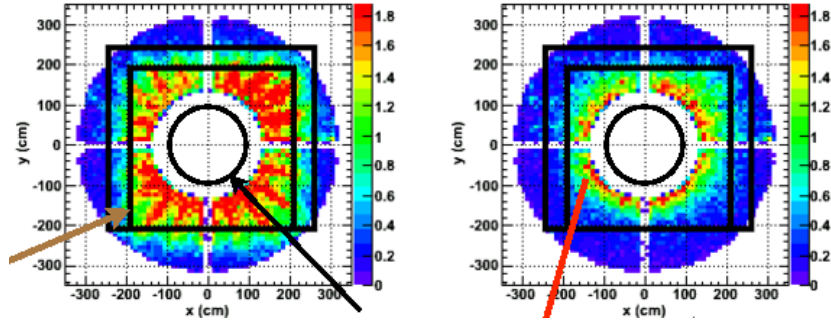


Figure 3.2.5: Background hit rate (Hz/cm^2) in the Belle KLM endcap before (left) and after (right) installation of polyethylene shield

3.2.3 Considerations at SuperKEKB

Because radiative Bhabha backgrounds scale are luminosity dependant they are a cause for concern for any high-luminosity upgrade design and will increase an order of magnitude with respect to KEKB. In addition the larger crossing angle of the nano-beam scheme will increase the transverse momentum of Bhabha particles when Lorentz boosted into the lab frame.

For the ECL, reduction of upstream quadropole bending combined with studies from quadropole magnet shielding predict background can be contained to negligible levels. A radiative Bhabha source will still pose the highest background for the KLM, however.

In order to properly assess the production of electromagnetic showers and neutron scattering in the IR it is necessary to complete the outer chamber and magnet designs, which should follow from the commencement of nano-beam SR background studies. In particular the chamber radius is reduced compared to KEKB due to the compaction of quadropole magnets, potentially intersecting with a greater range of Bhabha scattering angles.

3.3 Other Backgrounds

Studies of other beam background processes are not presented in this thesis will be vital for the operation of SuperKEKB and mentioned as follows.

3.3.1 Beam-Gas Scattering

Vacuum chambers only operate to a limited efficiency, and atoms from residual gas in the beam pipe interact with travelling electrons and positrons through Coulomb scattering and bremsstrahlung. Out of these, Coulomb scattering results in smaller changes in angles to the beam particles, whereas bremsstrahlung results in significant change to particle energy even in small path deviations.

Upstream beam-gas scattering which create showers from beam pipe collisions and affect many detector components is common to all accelerators. This background dependent on upstream vacuum level, beam current, beam optics and beam pipe dimensions is significant at KEKB. At SuperKEKB, it is also calculated that vacuum levels around the IP will be 100-1000 times greater than KEKB, potentially forming an extra source of background to inner detector components.

3.3.2 Touschek

Touschek scattering refers to the deviations in beam particle momentum due to intrabunch elastic scattering. Beta oscillation resulting in transverse motion collisions can produce longitudinal Coulomb scattering which becomes boosted in the lab frame. This results in path deviations similar to that from bremsstrahlung.

The extremely high density of particles in each bunch due to the nano-beam scheme will make this a major background at SuperKEKB. Rough estimations based on beam lifetime predict levels 20-30 times greater than those at KEKB.

Chapter 4

Synchrotron Radiation Background Simulation

4.1 Overview

In this chapter we present the simulation study conducted for a high-current optics based IR design. This design has since been discarded at SuperKEKB, however the tools and techniques shown here will be readily applicable to the continued study of SR background for the newly adopted nano-beam design.

In order to simulate SR hits from beam conditions, we generate particle data in two stages; event generation and geometry simulation. For each of the HER and LER beams, beam and magnet parameters are imported from the beam optics simulator *SAD* for use with a *Geant4* based beamline physics framework *LCBDS*, which is used to calculate the beam SR output. The generated SR data is then run through a separate beampipe geometry simulation in *LCBDS*. The IP chamber and detailed geometry model of the 25m surrounding IR beampipe is created to accurately determine the amount of backscattering into the IP chamber. In the analysis of results, data from both simulations are combined to tag the backscattered photons according to their generated origin and scattering vertex in order to determine background causes.

4.2 SR Event Generation

4.2.1 *SAD* Beam Optics Simulator

At KEK the main tool used for optimising beamline optics is the Strategic Accelerator Design (*SAD*) simulator, that has been featured in the development of many experiments including TRISTAN, KEKB, ILC and J-PARC. Among its

functions are matching of beam optics, geometry, off-momentum orbits, particle tracking, dynamic aperture and non-linear analysis. [15]

It does not, however, simulate the interaction of particles with physical material. By importing the beam and magnet parameters from those calculated by the SuperKEKB accelerator group, our aim is to separately recreate the design beam orbit in the IR for the background simulation study.

The LER and HER orbits are calculated in separate simulations. The particular parameters we import from *SAD* are:

- emittance in x, y
- beta and alpha (first derivative of beta) in x, y at the beam injection point
- dimensions and offsets of beamline components - steering, focusing, solenoid, drift space
- field strengths of magnets

4.2.2 *LCBDS* Beamline Simulator

The basis for our beam background calculations comes from the use of our *Geant4* based framework Linear Collider Beam Delivery System (*LCBDS*). [16] *LCBDS* is able to automatically create common beamline components such as drift spaces, steering magnets and quadropole magnets, align them along the correct beam orbit and output particular details of the simulation after running, allowing for the rapid prototyping of beamline configurations. It runs on top of the physics calculations of *Geant4*, a sophisticated simulation toolkit for particles passing through matter.¹ [17] *LCBDS* is not a released framework but supports many of the features required in replicating the simulation from *SAD*. Features that it does not support are continually being patched during its development.

After importing the beam optics parameters from the *SAD* optics the simulation is run for LER and HER, injecting electrons/positrons produced according to a 5σ random gaussian beam profiles at the first upstream bending magnet. Tail particles outside this range would likely prove important for runs at high statistics, however require greater study of non-linear distributions yet to be performed in our simulation. SR photons are generated by the *Geant4* code along the orbit and their position and momenta saved to file. Magnetic field trajectories can be computationally intensive and for the generation of events comparable to one beam bunch (1×10^{11} for the LER and 0.5×10^{11} for the HER) can take weeks on a 400 core cluster. Pregenerating the SR data and saving to file allows for changes in in subsequent beampipe geometry simulations to be implemented more flexibly.

¹Note that our geometry simulation requires use of *Geant4* 9.1 and up due to boundary interpretations problems in previous versions

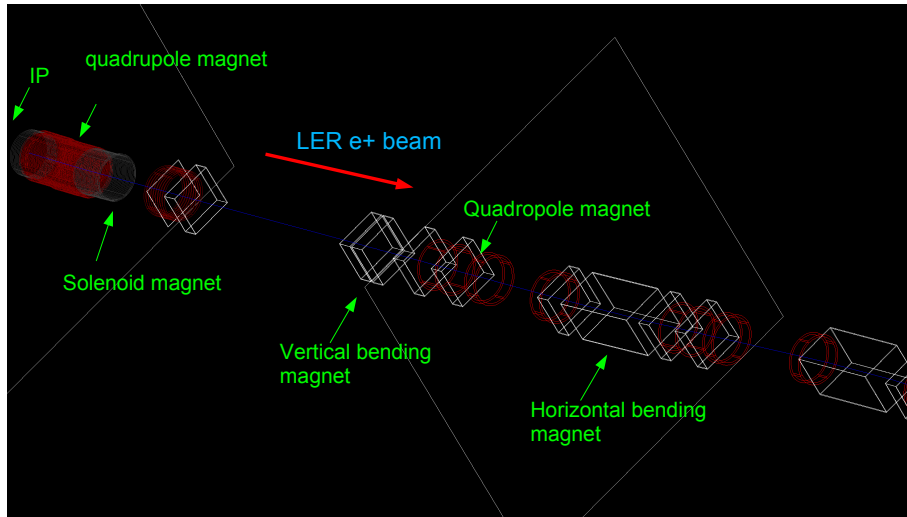


Figure 4.2.1: Example of a positron track in a beamline structure created in *LCBDS*

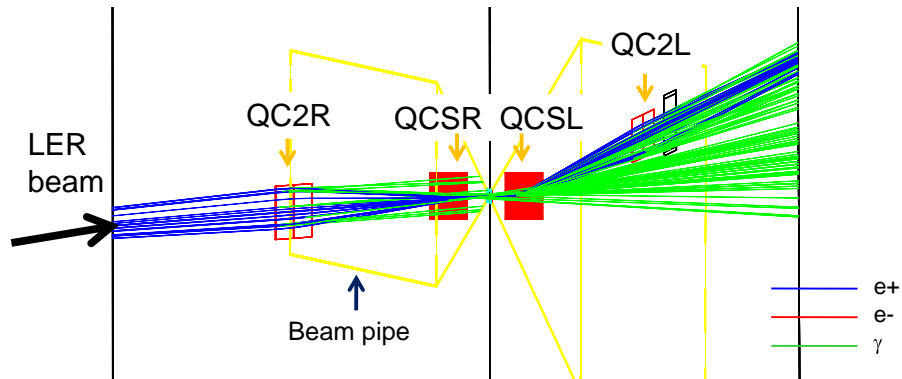


Figure 4.2.2: SR emitted from LER beam passing through quadrupole magnets in the IR (IP chamber geometry included)

4.3 Beampipe Scattering Simulation

The second stage in simulation is to run the generated SR events with a full IR beampipe geometry model again in *LCBDS*, with the magnetic fields removed. The beampipes for the LER and HER were created separately, both sharing the same IP chamber model. Beampipe dimensions were taken from CAD files, and included much non-trivial geometry for which a tessellation-based algorithm was written to accurately represent it. Specifically angled joints and widened

oval-shaped beampipes are featured along the downstream designed to avoid SR fan regions, and the model code automatically generates and connects each section without gaps or overlaps.

To save CPU time, SR input events are first filtered to discard tracks of low energies since they are unlikely to penetrate the IP chamber (see section 4.4).

During the simulation *Geant4* detects collisions of SR photons with the beampipe and calls the appropriate scattering or absorption process. Any secondary particles emitted are likewise tracked until all particles are absorbed or leave the pipe. The chain of energy deposit data is outputted by *LCBDS* to file.

4.3.1 Beampipe Model

4.3.1.1 IP Chamber

The IP chamber model consists of a 12 cm long, 1.5 cm inner radius pipe with 2 mm thickness of beryllium and 10 μm gold inner layer. At the entrance of the HER upstream there is a circular gold SR mask with 4mm height designed to shield forward SR from the chamber. Attached to both ends are 5mm thick conical gold shields which taper out at 30 mrad, overlapping with the outer IR beampipe

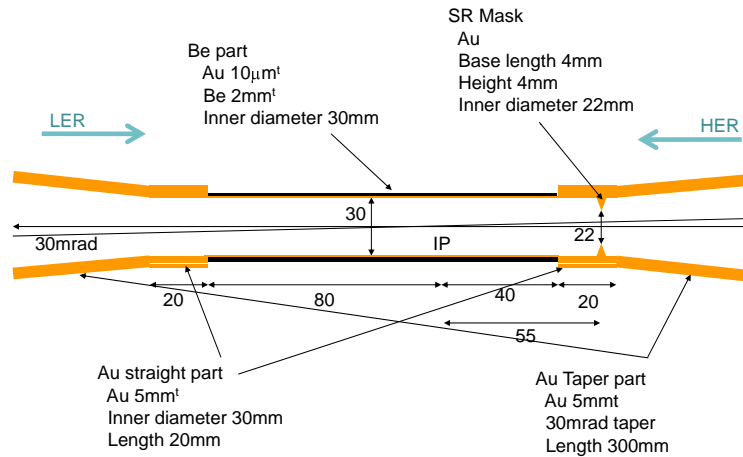


Figure 4.3.1: Diagram of the IP chamber model

4.3.1.2 Outer IR Beampipe

The IR beampipe material used for the main analysis of the simulation was a combination of 6mm thick copper with an inner layer of 10 μm gold. A single aluminium pipe was also simulated for comparison.

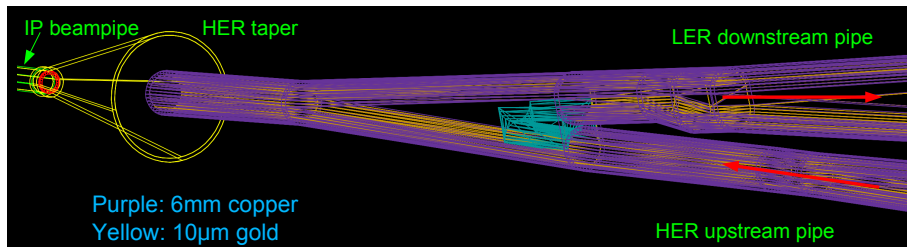


Figure 4.3.4: LER downstream model in *LCBDS*

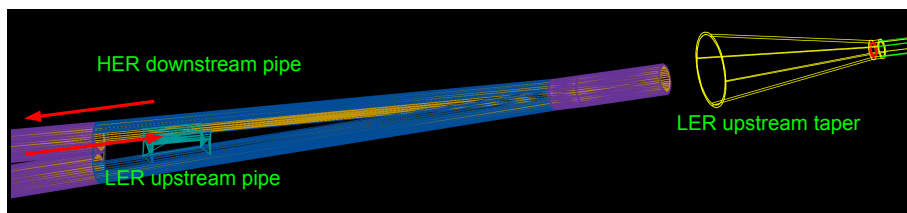


Figure 4.3.5: HER downstream model in *LCBDS*

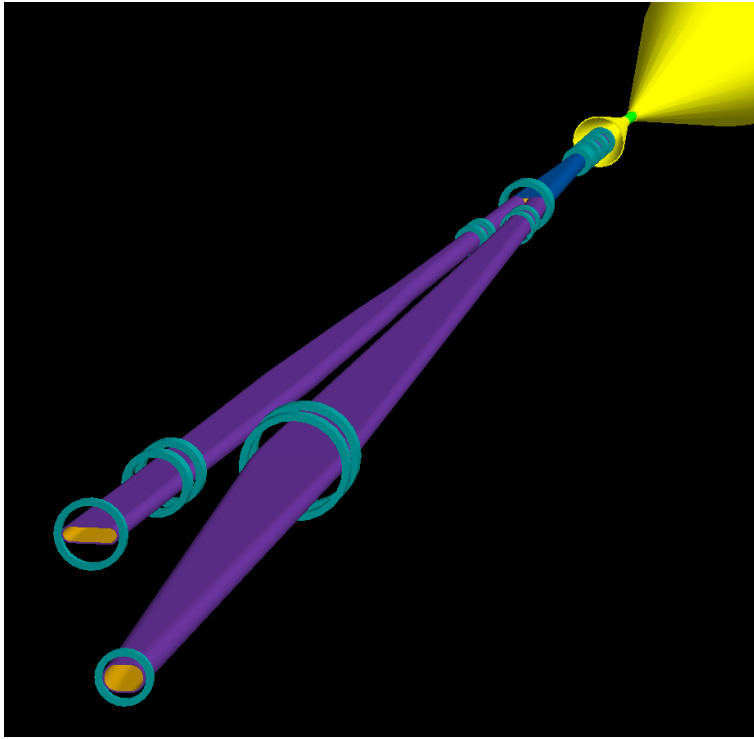


Figure 4.3.6: Solid visualisation of the LER downstream beampipe (with approximated flanges attached)

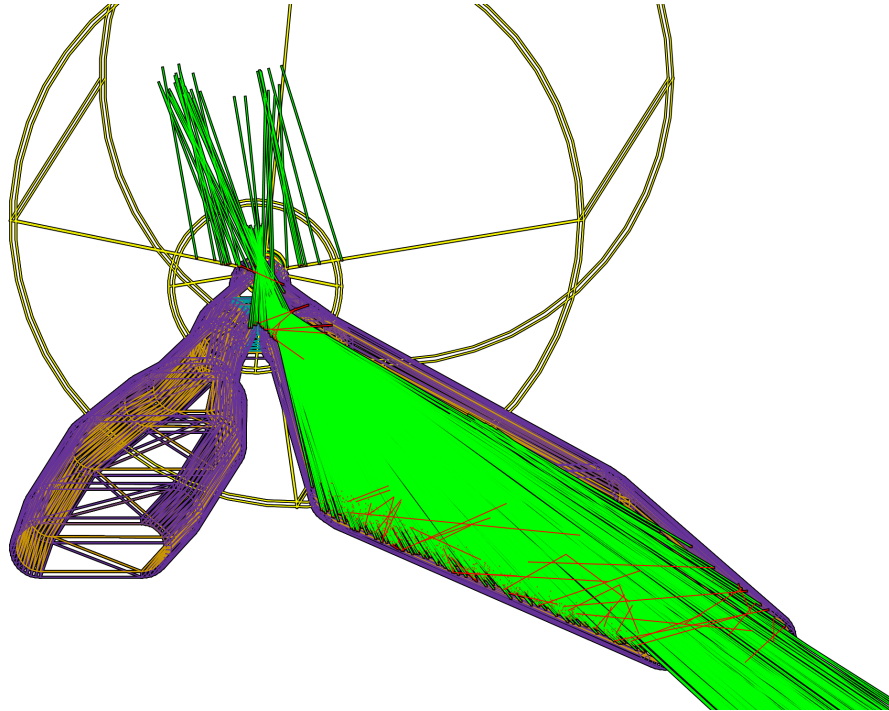


Figure 4.3.7: View of SR colliding with the LER downstream beampipe to produce secondary particles; red tracks are electrons

4.3.2 Limitations of two-stage simulation

By avoiding the insertion of magnetic fields into the beampipe simulation the computation time is reduced significantly. Some limitations exist when separating the simulation into two stages however:

- Many secondary-produced compton and photo electrons are generated during hits to the pipe. In the beampipe simulation these electrons are not bent by the quadropole fields and hence do not produce any SR. Their energies however are far lower than these of the beam and so this contribution to the background can be considered negligible
- The number of scattered electrons is far greater than scattered photons, and many will enter the IP chamber. Their low transverse momentum suggests that the longitudinal magnetic field from the detector solenoid will cause them to spiral uneventfully through the IP chamber without ever hitting the wall. This principle was tested by selecting secondary electrons backscattered near the chamber and running them with the Belle II solenoid field included. The result was no hits to the IP chamber.

4.4 PXD Occupancy

The DEPFET Pixel Detector design in Belle II has an integration time of $\sim 10\mu\text{s}$, until which a pixel is said to be occupied. The operational preference is for the occupancy level of the 2.7 million pixels to not exceed 1% at any one time, a limit of 27k hits per event. In terms of a beam bunch circulating at 500 Mhz this limit is then equal to $27\text{k}/5000 = 5$ hits per bunch.

From simulations of photons incident at 30 mrad, shown to be the average for particles entering the IP, on to the the gold/beryllium chamber it was shown that for high energy $50 \sim 100$ keV photons around $5 \sim 10\%$ will penetrate into the PXD layer (figure 4.4.1).

Hence we determine that the threshold level for background high energy photons posing PXD occupancy problems is ~ 50 incident IP chamber hits per beam bunch.

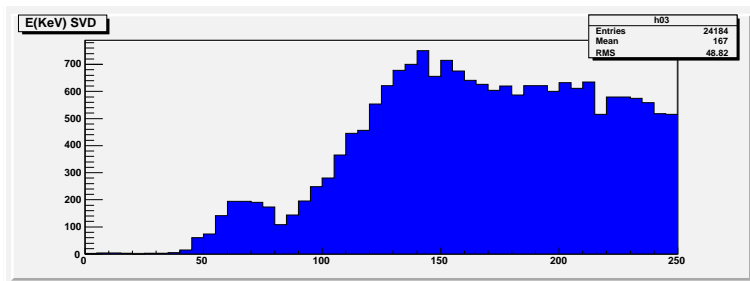


Figure 4.4.1: PxD energy deposit simulation for 30 mrad incident photons inside a Be/Au IP chamber (bottom axis is photon energy in keV)

4.5 Simulation Analysis

4.5.1 Total Energy Deposits from SR

4.5.1.1 Study of Previous Optics from 2008

Two proposals of the high-current scheme were simulated during the study. The first optics was current to 2008 and based on the Letter of Intention design with modifications for beam-beam limits. We present results from this study to comment on how changes to optics from 2009 affected SR background.

LER

25 million LER positrons events equivalent to $1/400$ of a beam bunch were run through the optics simulation. From this a cut of $E_{SR} > 1$ keV was placed on the generated SR and run through the beampipe simulation.

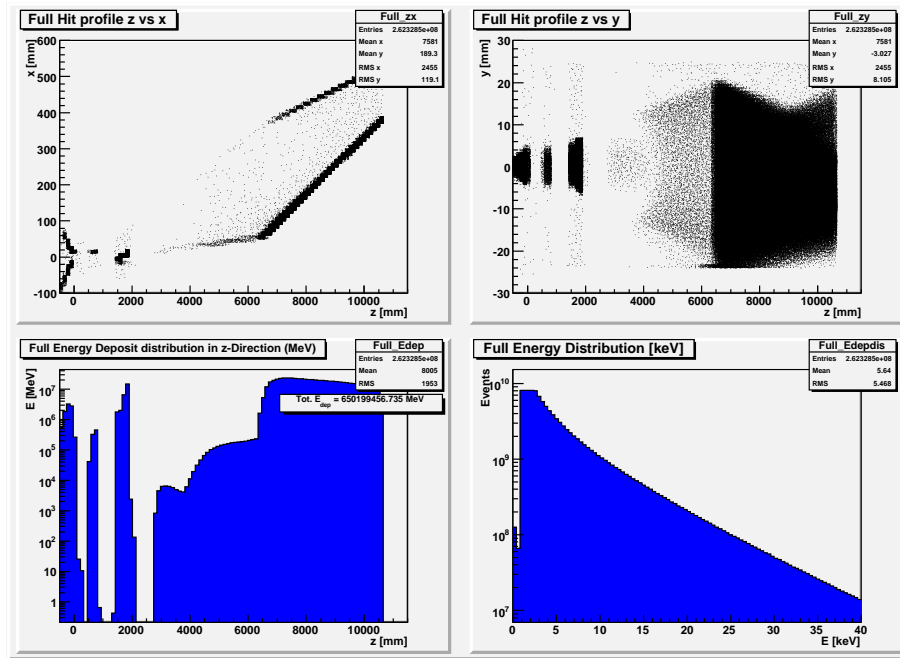


Figure 4.5.1: 2008 Optics SR energy deposit from the LER in the full downstream pipe. For all plots values scaled to one beam bunch. IP is at 0

In figure 4.5.1 the top two plots are the z vs x and y hit profiles in the LER downstream beampipe, for all hits including those from scattered secondary particles. All values are scaled to single beam bunch values. The IP is located at 0 in these profile plots. It can be seen that the shape of the downstream pipe allows many hits to pass until the end pipe region after 6m downstream. The energy spectrum of the SR is shown in the bottom right graph, and is seen to be low, falling under 40 keV.

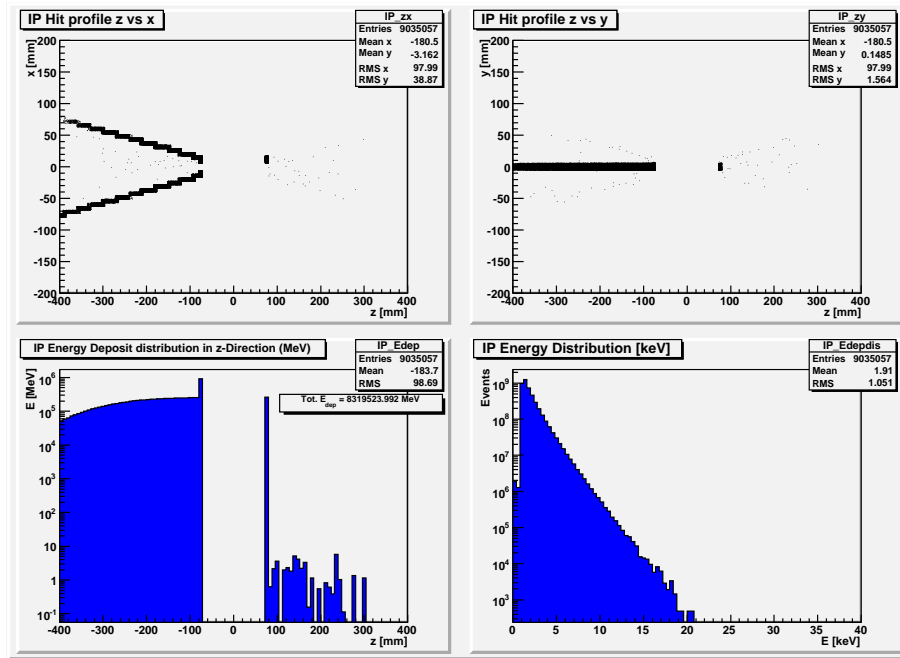


Figure 4.5.2: 2008 Optics SR energy deposit from the LER near the IP

Figure 4.5.2 focuses on the ± 40 cm region around the IP. In the x profile the hits to the the gold upstream taper shield is clearly seen. SR energies are very low. For the event size used in the simulation no hits were seen to the IP chamber.

HER

25 million electron events equivalent to $1/200$ of a beam bunch were used in for the HER simulation. A larger cut of $E_{SR} > 20$ keV was used due to the increase in photons generated by the HER beam.

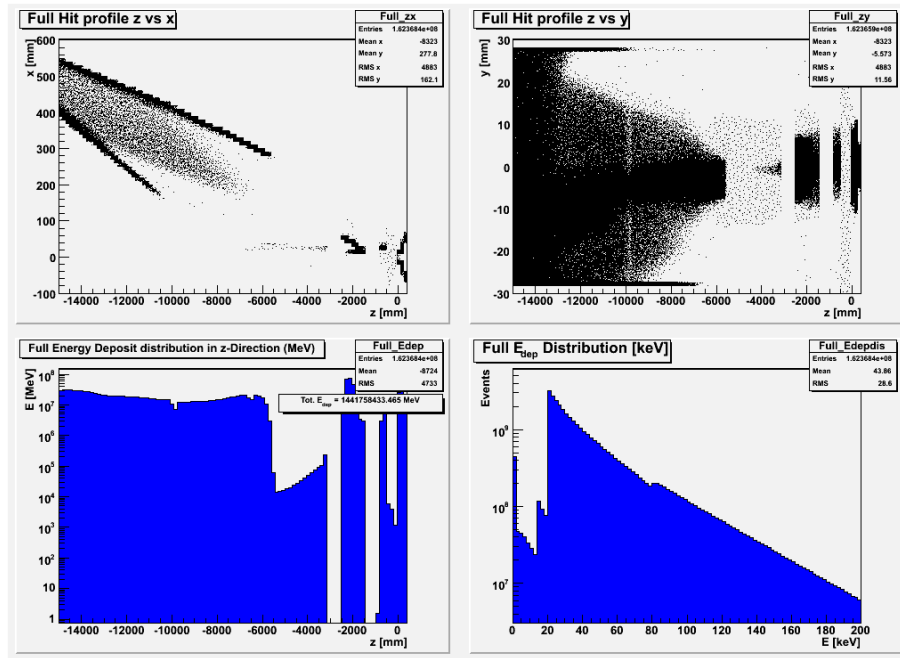


Figure 4.5.3: 2008 Optics SR energy deposit from the HER in the full downstream pipe

In figure 4.5.3 the spectrum of energies can be seen to increase dramatically, as the higher beam energies increase the critical SR energy by E_{beam}^3 . The spectrum below the filter cut of 20 keV are from secondary particles.

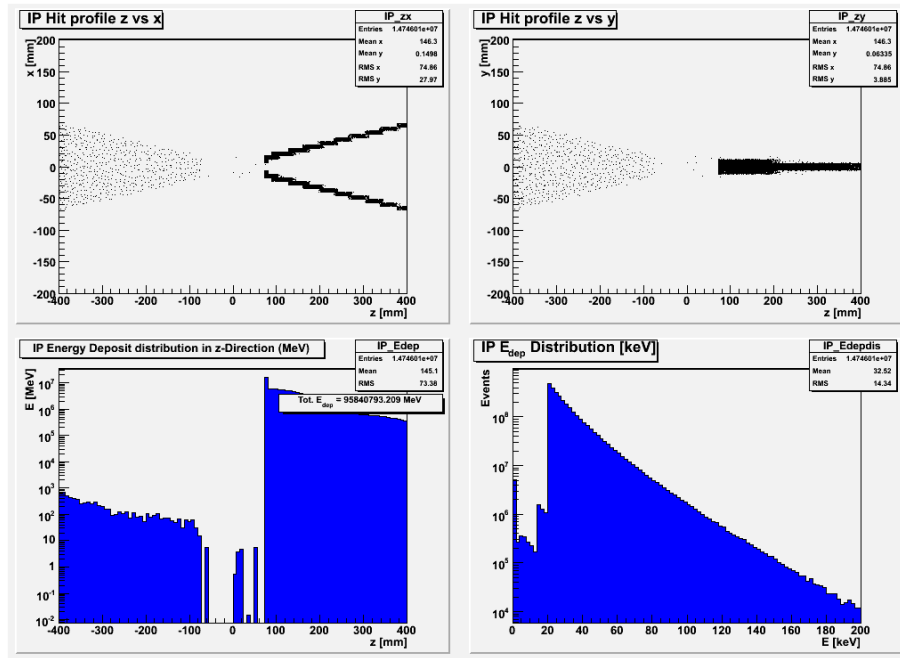


Figure 4.5.4: 2008 Optics SR energy deposit from the HER near the IP; note that hits in the chamber region are exaggerated due to the absence of solenoid field

The IP region is shown in figure 4.5.4. The energy spectrum is very high with energies above 100 keV, and this can be seen in high +1 kW energy deposits to the SR mask (seen in the spike before the IP chamber in the bottom left plot). Although in this plot there are multiple hits recorded in the IP chamber, only one of these is a photon as seen after filtering for photons only in figure 4.5.5, of low energy ~ 30 keV. As we will show in 4.5.2, this photon was backscattered from the downstream pipe. The rest of the hits are due to secondary electrons, which when resimulated with the Belle II solenoid field included were found to clear the IP chamber.

Applying the statistics used in the simulation the result then is tentative 200 low-energy hits per bunch to the IP chamber. Much higher statistics would be required to measure SR background for this optics design with greater confidence.

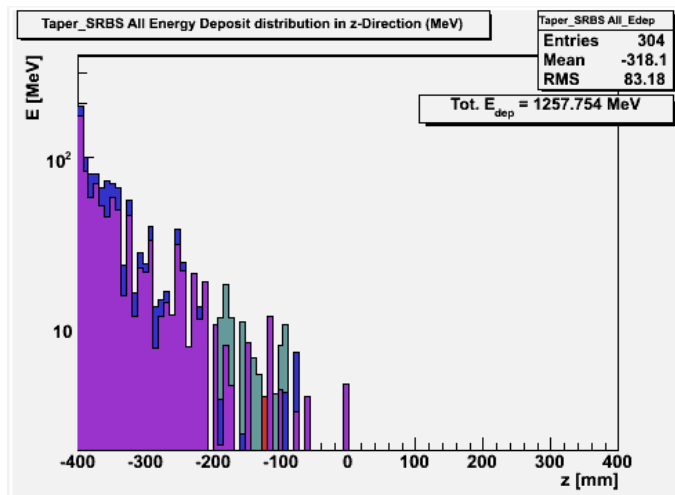


Figure 4.5.5: 2008 Optics photon energy deposits from the HER around the IP chamber. The equivalent of 200 hits per beam bunch are seen close the to IP (colours represent SR origin; see section 4.5.2)

Summary of Beampipe Heating

The total power deposited for the LER and HER downstream pipe regions are summarised in figures 4.5.6 and 4.5.7. These values are manageable by the use of suitable cooling systems in the chamber and not problematic.

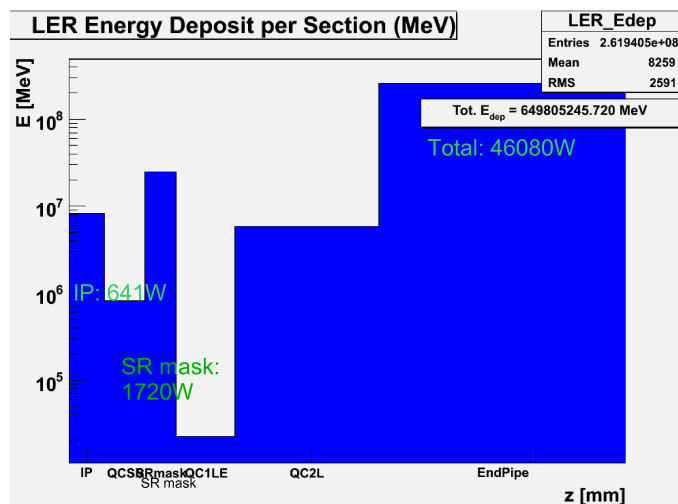


Figure 4.5.6: 2008 Optics SR deposit summary for the LER downstream IR

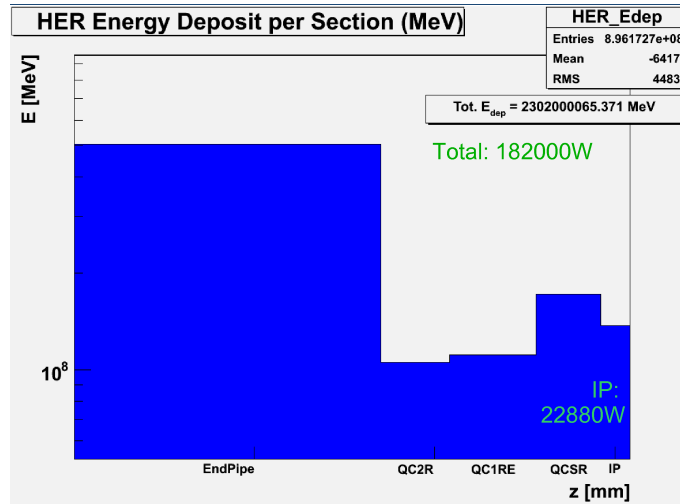


Figure 4.5.7: 2008 Optics SR deposit summary for the HER downstream IR

4.5.1.2 2009 Optics (1012a)

In February 2009 a new high-current beam optics design (1012a) was released by the SuperKEKB accelerator group, moving the magnets closer to the IP and introducing an additional permanent QCS quadrupole magnet in the HER upstream (shown in figure 3.1.5). The beam size at the QC1 quadrupole magnets was reduced to half of the previous optics.

In light of the SR simulation results from previous optics we focused our study on the HER beamline. An initial run of 50 million electrons with the new optics was repeated in the simulation, with a $E_{SR} < 20$ keV cut placed on SR events.

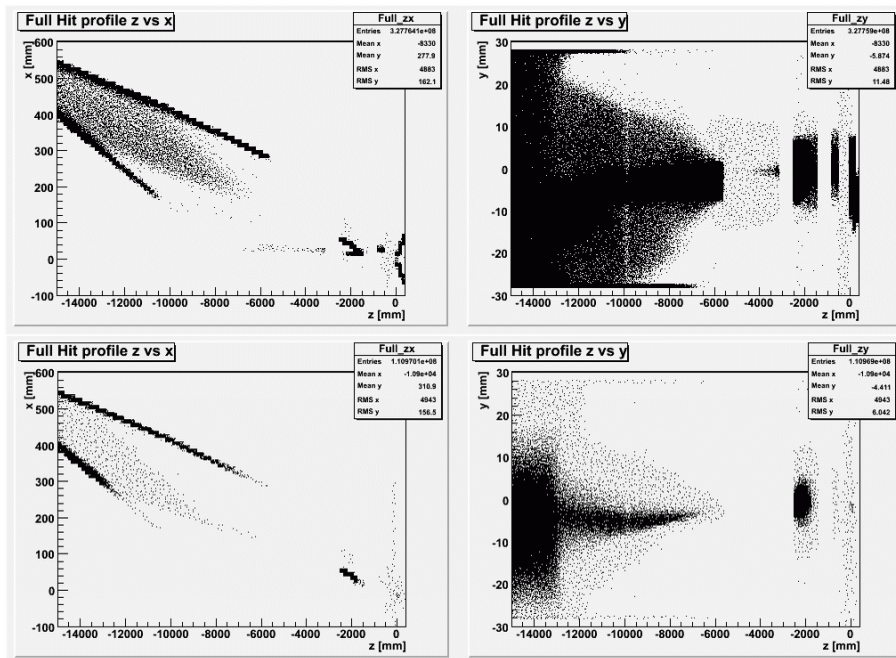


Figure 4.5.8: Comparison of SR deposits in HER downstream for 2008 (top) and 2009 (bottom) optics, with cut $E_{SR} < 20$ keV. The number of hits is reduced to 1/3 in the new optics

Figure 4.5.8 compares the x and y hit distributions for the 2008 and 2009 optics. The number of hits is reduced to 1/3, and the y distribution appears significantly narrower. Notably, the problematic 1 kW of heat deposited to the HER SR mask was seen to be reduced to 100 W, a high but now manageable quantity.

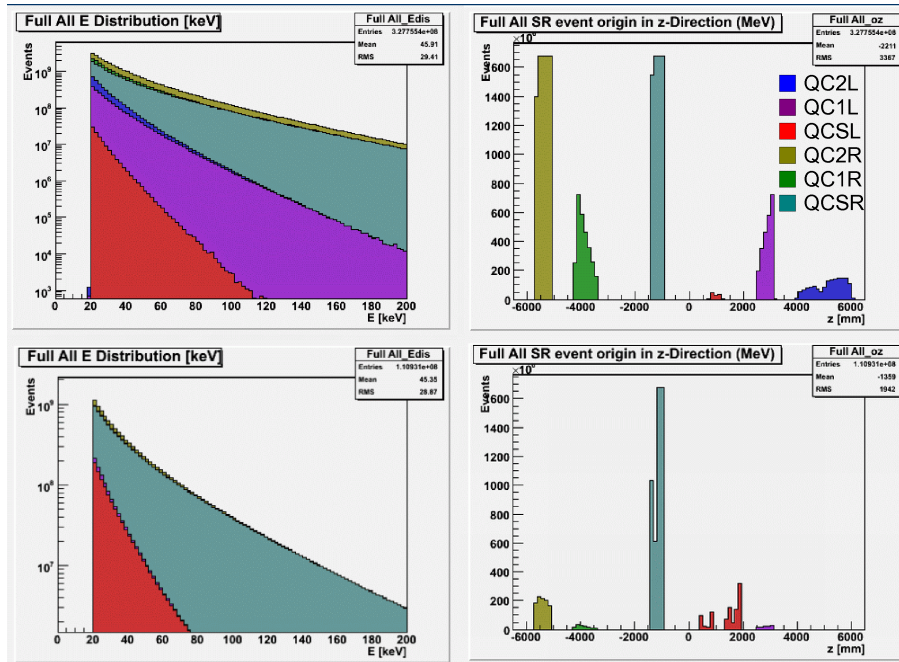


Figure 4.5.9: Comparison of HER SR energy distribution and SR production origin for 2008 (top) and 2009 (bottom) optics

In order to study the origins of SR deposits, we cross-reference the hits with the SR event data and colour-code the histograms according to which magnet the SR was produced in. We can see from the comparison of 2008 and 2009 optics in figure 4.5.9 that the amount of SR produced from the QC1 magnet has dropped remarkably due to the beam size reduction. This was important as previously the majority of backscattered photons near the IP in figure 4.5.5 originated from this magnet. Production from the upstream QC2 magnet also decreased dramatically. SR energies from the QCS upstream are higher however (y -axis scales are different in the two energy distribution plots), with contributions from the extra QCS permanent magnet in the design (red areas include both permanent and superconducting QCS upstream magnets). In both plots we can see that the bulk of the high energy spectrum is due to high-bending in the upstream QCS region.

At these statistics of 1/100 of a bunch there were no hits seen to the IP chamber. The 2008 optics study suggested that the source of any hits to chamber would come from backscattering, and we focused our study on this effect for the larger data samples.

4.5.2 Backscatter SR Analysis

4.5.2.1 Track Selection

Aiming to create as close to one beam bunch as feasible, we generated SR events from the 2009 optics over approximately 3 weeks in total for HER and LER using the 400 core computing facility at KEK. The bottleneck ending up being the transfer of data back to the computers at The University of Tokyo. Utilising an automated batch scripting system the transferred event data was filtered for $E_{SR} > 5$ keV and run in parallel with the beampipe simulation on our local cluster. Tracks which hit the IP chamber plus tracks backscattered off the beampipe were then saved for the analysis. Backscattered tracks were selected by requiring their longitudinal momentum to opposite that of the incoming beam, regardless of the distance travelled from the original SR scattering vertex. This meant that deposits from scattering inside the beampipe material also appear in the data, but this was not ruled important for the overall analysis.

4.5.2.2 HER

25 billion electrons, the equivalent of half a beam bunch, were simulated in HER IR for our final calculation. The backscattered hits near the IP are shown in figure 4.5.10. From the top left plot we can see the two largest contributors to backscattered photons which reach within 40 cm of the IP were the upstream and downstream QCS magnets (SR from QC2 (blue) can be seen to scatter off the upstream taper shield). The top right plot is the distribution of the scattering vertex (where the original SR photon first hits) along the beampipe. The backscattering occurs at ~ 2 m past the IP near the QCS magnet and ~ 14 m at the far end of the IR where the beampipe radius converges.

The result is one simulated hit (equivalent to 2 hits per beam bunch) made to the IP chamber, resulting from SR produced from the QCS magnet backscattering 2 m downstream. This was a low-energy deposit of 40 keV and absorbed by the chamber. This result clearly that HER SR background has little risk of significantly contributing to PXD occupancy in this beampipe configuration.

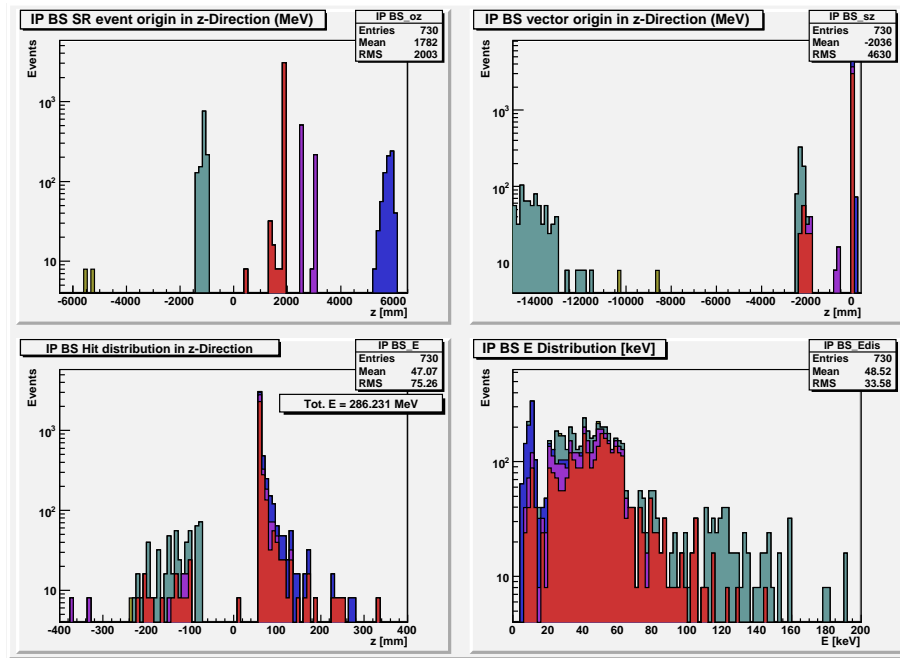


Figure 4.5.10: Backscattered SR near the IP from the HER

4.5.2.3 LER

For the LER we ran 5 billion positrons in the optics simulation, equivalent to 1/20 of a beam bunch. Despite the level of statistics, after filtering SR events for $E_{SR} > 5$ keV the data is reduced to 1/7 of the original amount, and the final number of backscattered photons in the entire beampipe simulation is just two, both near the IP (figure 4.5.11). This can be explained by photoabsorption being the dominant process in gold with its high atomic number $Z = 79$, and for the low-energy SR in the LER no K or L edge emissions follow since K edge energy in gold is 80 keV. SR from the LER can be seen to be of sufficient low-energy as to not pose a background in this IR.

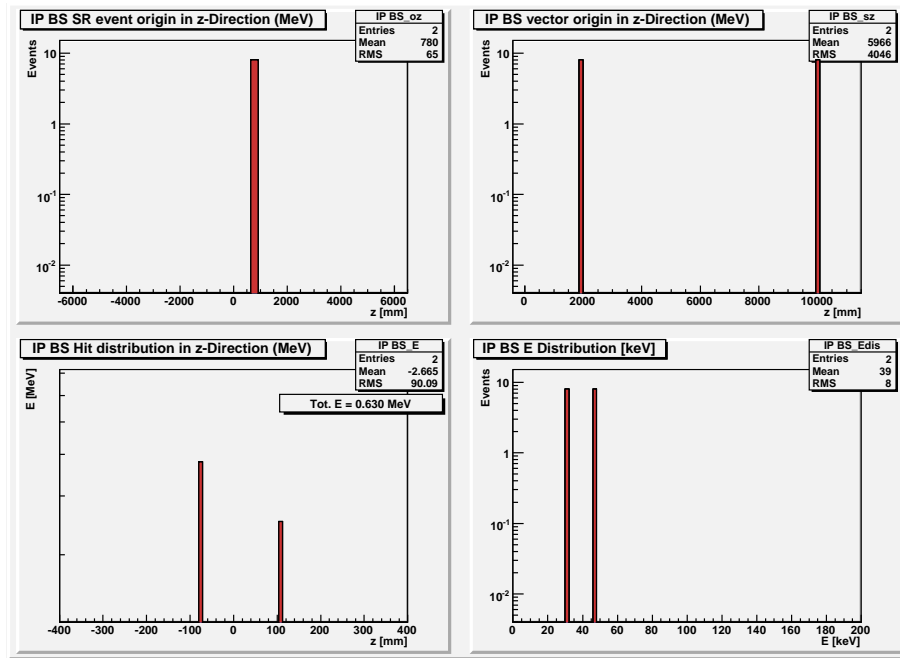


Figure 4.5.11: Backscattered SR near the IP from the LER

4.5.2.4 Aluminium HER Downstream Beampipe

We additionally simulate SR backscattering from the HER in a pure aluminium downstream beampipe, with statistics of 1/10 of a beam bunch and SR cut of $E_{SR} > 5$ keV. Resulting backscattered hits near the IP are shown in figure 4.5.12. Overall the amount of scattering and the energy range of scattered photons is increased compared to the Au+Cu beampipe, including an appearance of some low-energy photons originating from the QC2 upstream magnet. Aluminium, while cheaper and simpler to manipulate than gold or copper, has a significantly lower atomic number $Z = 13$, leading to increased rates of compton scattering of high-energy x-rays. K edge emission yields from photoabsorbtion are small in Aluminium however and of low-energy. The equivalent of 30 hits are seen to the IP chamber, again mainly from QCS upstream but also QCS downstream, which is of concern due to its higher energy spectrum. For this optics design aluminium significant increases the rate of PXD background.

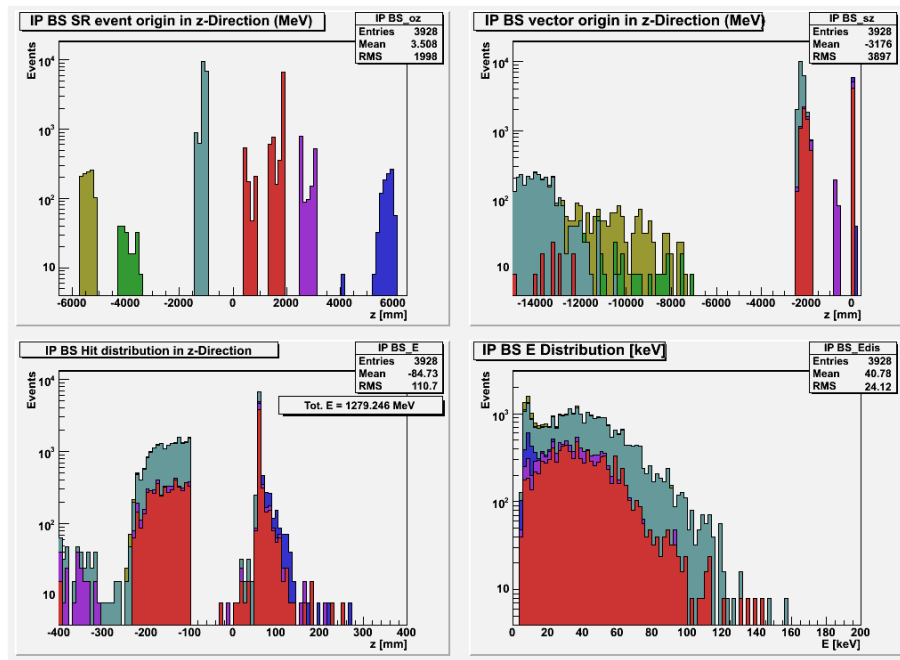


Figure 4.5.12: Backscattered SR near the IP from the HER with an aluminium beampipe

Chapter 5

Radiative Bhabha Background Simulation

5.1 Overview

The goal of this study was to set up the foundations for a full calculation of radiative Bhabha related background at SuperKEKB. Exact determination of electromagnetic showers and neutron scattering in the IR requires realistic modeling of the beampipe, quadrupole and steering magnet physical structure. We instead perform a statistical evaluation of whether the upstream QC1 fields from the nano-beam design directly bend off-momentum particles into the detector region. The tools to test this will be the same as those required in future radiative Bhabha simulation studies.

The simulation takes place again in two stages. Event data for Bhabha small angle scattering is generated using the Bhabha simulator *BHLUMI* in the CM frame, with an angle cut placed according to the dimensions of the IR layout. This data is then Lorentz boosted into the lab frame and run through an IR simulation in *LCBDS*, incorporating a geometry setup consisting of the IP chamber and Belle II detector, and quadrupole magnetic fields imported from the *SAD* nano-beam lattice.

5.2 Radiative Bhabha Event Generation

5.2.1 *BHLUMI* Bhabha Simulator

BHLUMI is a Monte Carlo program for small-angle Bhabha scattering incorporating radiative and Z resonance corrections, with a claimed overall precision of 0.11%. [18] This program will generate momentum for final state electron,

positron and photons for a definable angle subrange and calculate the cross-section for the process.

We choose a minimum scattering angle which corresponds to the exit of the QC1 quadrupole magnet (which is the closest magnet to the IP in the nano-beam and plays the role of the QCS) at the radius of the gap (1 cm), and a maximum angle corresponding to the entrance at the radius. This way we are able to maximise statistics for the region of tracks we are interested in.

Because *BHLUMI* calculates the interaction in the CMS, these angles must be rotated and Lorentz boosted before passing them into the program. Similarly, momentum values from the *BHLUMI* event output must be rotated and Lorentz boosted into the lab frame before running them in the IR beamline simulation.

5.3 Beamline and Detector Modelling

5.3.1 Beamline Structure

The *SAD* optics lattice used in the simulation was constructed with no solenoid field, so we include only the four quadrupole fields in each of the LER and HER beamlines. The crossing angle in this design is much smaller at 30 mrad. The beampipe is based on rough estimations at the time and incorporates the symmetrical straight IP chamber connected to “V” pipes on both sides. Due to limitations in visualisation output in *Geant4* the V components appear to be boxes in the figures, but they are actual pipes in the physics simulation.

5.3.2 Belle II Detector

The implementation of the Belle II detector serves as a solid mapping of the main components. The particular interaction with the detector is not important, only the entrance and energy of the deposits.

The new PID in Belle II is installed into the barrel and endcap, and shares a similar risk to radiative Bhabha background as the ECL. The CDC, PID and ECL are included in the simulation model. The KLM was not added due to absence of any neutron scattering simulation.

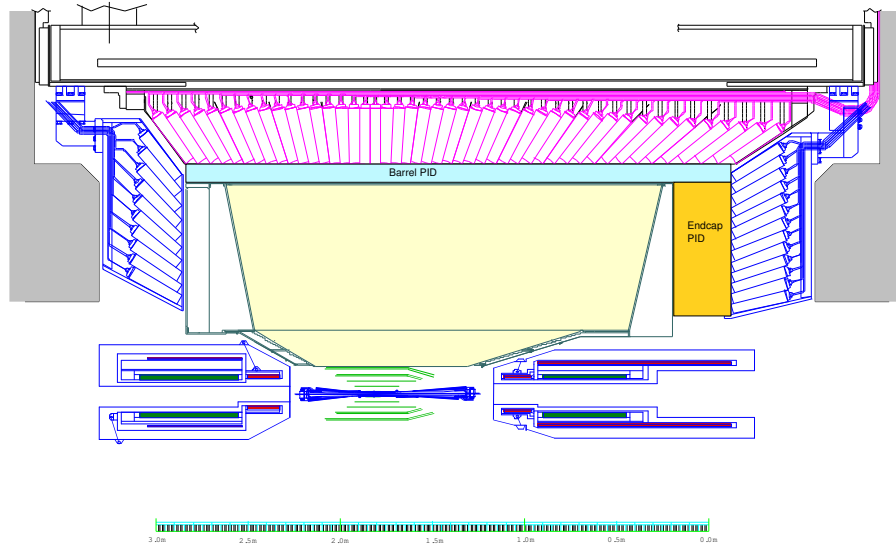


Figure 5.3.1: Diagram of the Belle II detector (IP chamber is for the high-current design)

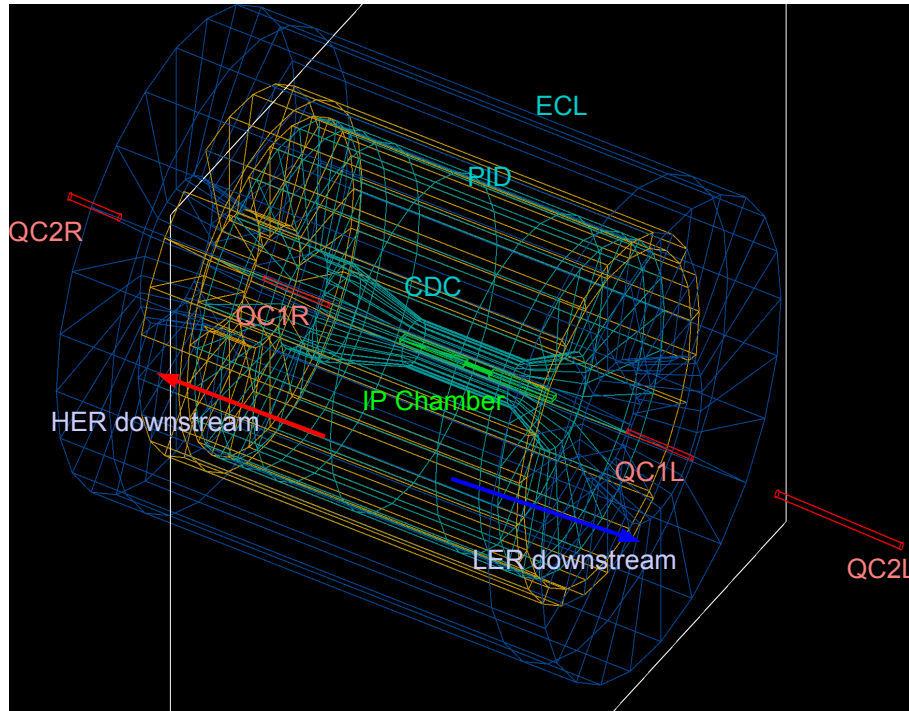


Figure 5.3.2: Model in *LCBDS* of the HER beamline and Belle II detector

5.3.3 Event Filter

In addition to transforming events to the lab frame, a more precise angle cut is placed on the data before simulation as *BHLUMI* does not strictly adhere to the input angle limits. This ensures that no hits are made the beampipe prior to passing through the QC1 magnet - such hits are expected to be shielded from the detector from the heavy metal shields stretching out from the IP chamber. Photon events are also cut as there is no KLM background determination in the simulation.

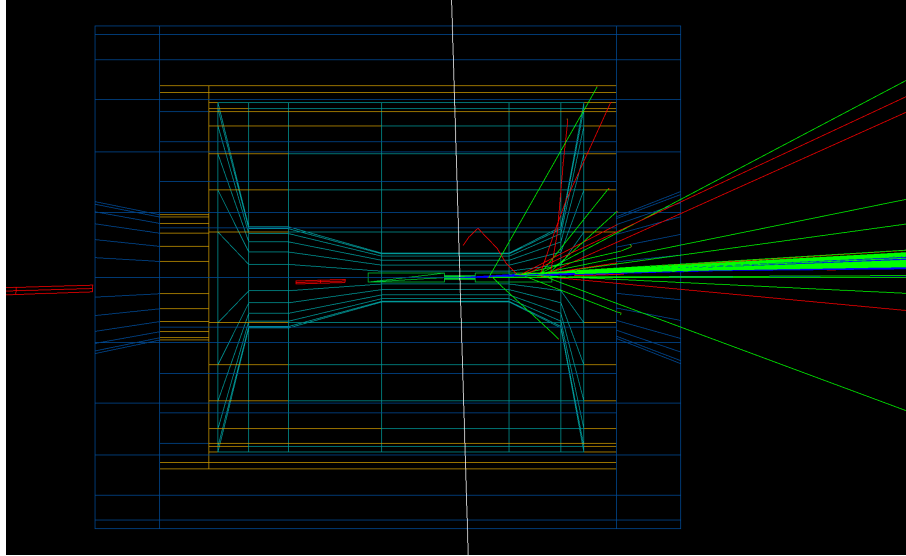


Figure 5.3.3: Run in the LER beampipe showing beampipe hits without an angle-cut

5.4 Simulation Results

10 million radiative Bhabha events were generated within a angle range of 4.5 to 13.5 mrad, corresponding to a cross-section of 0.3×10^{-3} nb. This is the equivalent of 1000 beam bunches at full luminosity.

The result for both LER and HER beamlines was no direct bending of particles into the detector. Typical bending trajectory and the emission of SR can be seen in figures 5.4.1 and 5.4.2.

Although larger-crossing angles in the recent nano-beam optics designs would contribute to transverse momentum, the statistics from this simulation demonstrate that low-angle events maintain ample longitudinal momentum to avoid direct bending paths into the detector.

The next step to determine ECL,PID and KLM scattering background is to realistically model the beampipe and QC1 physical structure.

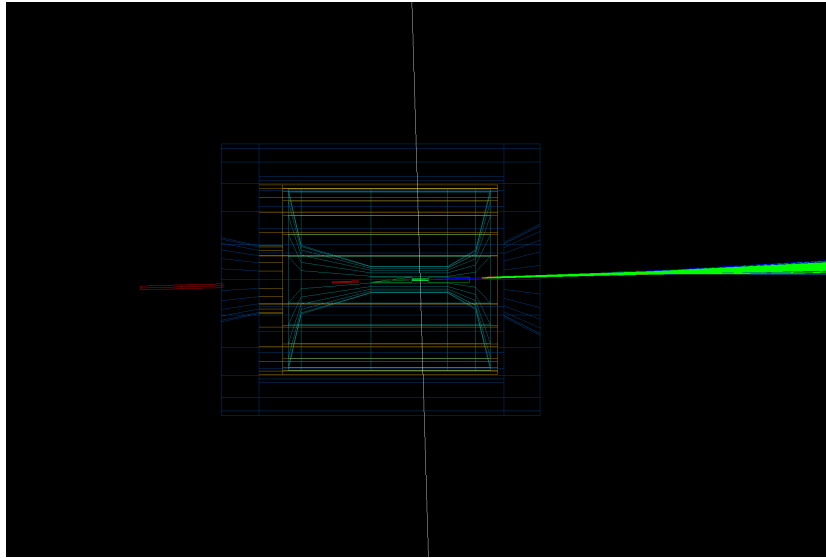


Figure 5.4.1: Visualisation of Bhabha events in LER beamline

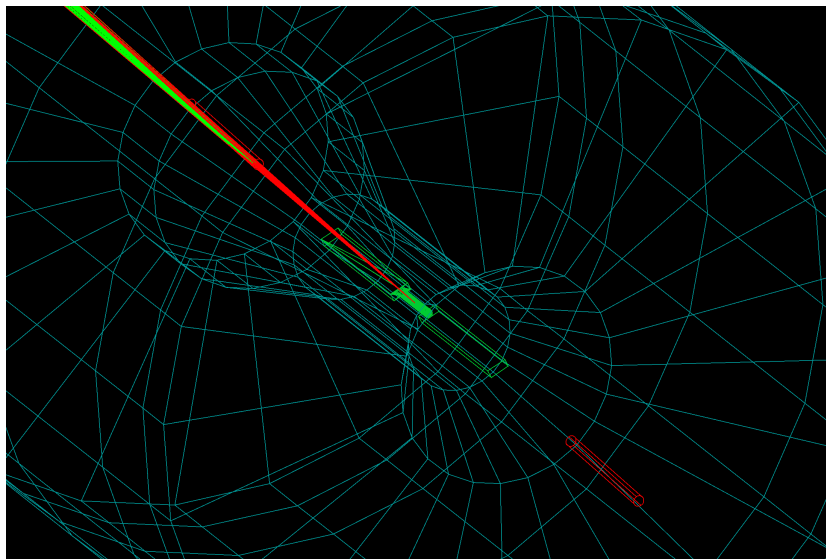


Figure 5.4.2: Visualisation of Bhabha events in HER beamline

Chapter 6

Further Work and Projects

A number of further background studies will be possible to implement using the same underlying IR simulation technique in this research.

The foremost of these includes beam-gas interactions which is expected to be one of the main beam-induced backgrounds in the new nano-beam design. Design of the IR chamber is a priority to all studies of the IR, and hence nano-beam SR simulations are critical as they will offer suggestions to shape the geometry and install masks.

These simulations hinge on the function of an accurate *Geant4* nano-beam optics simulation. Work into implementing recent IR nano-beam optics designed in *SAD* progressed steadily over the final course of this research, but unfortunately met with apparent numerical integration problems inherent to tiny trajectories. These must invariably be overcome before advancing the study in earnest. The solution may possibly involve creating new path algorithms as the Runge Kutta method used by *Geant4* has been shown to produce anomalies in the past.[16]

To test the simulation method, a simulation of current KEKB IR beamline structure should be run and compared to experimental detector data.

Finally, the SuperKEKB and Belle II design, and in particular the recently adopted nano-beam optics, are still far from their final stages of conception, and IR background simulations must be continually revised as part of the interplay between IR design and testing. It is for this purpose that a flexible simulation testbed is important in studies also, which has been given mind to from day one in this research. Equally as important will be the documentation of such methods, one which the *LCBDS* framework could make a much simpler task one day.

Chapter 7

Conclusion

A simulation study of synchrotron radiation background in a high-current based accelerator design and radiative Bhabha background in a nano-beam based design for SuperKEKB was performed.

SR simulated from 0.5 (HER) and 0.05 (LER) beam bunch samples was tracked inside a realistic IR chamber model, resulting in an estimated number of 2 low-energy backscatter SR hits per HER bunch to the IP chamber and effectively no hits from the LER. This number is significantly less than the estimated 50 hit limit occupancy requirement of the PXD. A combination of IR chamber geometry, material and beam optics layout can be said to mitigate the problem of SR background at a high-current optics scheme.

Radiative Bhabha events equivalent to 1000 bunch collisions were tracked inside an preliminary nano-beam IR model. Particles were shown to have no tendency to undergo direct bending paths into the detector. EM showers and secondary neutrons are the only candidates for this background, which can be determined with the inclusion of outer IR structure in simulations.

The simulation methods employed in both of this studies can be used to continue SR and radiative Bhabha background modelling through the course of SuperKEKB's IR design, in particular to give feedback on the the nano-beam scheme which has become the centrepoint to achieving the project's luminosity goals.

Chapter 8

Appendix

8.1 Flavour Properties of Kaluza-Klein States

The various models of extra dimensions proposed today extend from the basic states arising in Kaluza-Klein excitation. Kaluza-Klein theory was originally developed to unify gravity and electromagnetism into a single geometrical framework. [6] In the theory, an extra spatial dimension is “compactified” into a circle of extremely small radius of order the Planck length. Observers trapped on the four-dimension “brane” are unable to probe this higher-dimensional space known as the “bulk” without overcoming the brane tension. A five-dimensional spacetime is what allowed for the separation of four-dimensional gravitation plus an extra set equivalent to Maxwell’s equations for the electromagnetic field. The five-dimensional representation is given by

$$\hat{g}_{\hat{\mu}\hat{\nu}} = e^{\phi/\sqrt{3}} \begin{pmatrix} g_{\mu\nu} + e^{-\sqrt{3}\phi} A_\mu A_\nu & e^{-\sqrt{3}\phi} A_\mu \\ e^{-\sqrt{3}\phi} A_\nu & e^{-\sqrt{3}\phi} \end{pmatrix} \quad (8.1.1)$$

where $\hat{u} = 0, 1, 2, 3, 4$. Combined with $\hat{R}_{\hat{\mu}\hat{\nu}}$, the theory correctly recovers for $g_{\mu\nu}(x)$, $A_\mu(x)$ and $\phi(x)$ fields the Einstein equations for a spin 2 graviton, Maxwell equation for a spin 1 photon and massless Klein-Gordon equation for a spin 0 dilaton. [7]

The periodicity of the compactified extra dimension allows its Fourier expansion to create an infinite n series of fields with identical quantum numbers in four dimensions, known as the Kaluza-Klein tower. On the brane these masses are given by $m^{(n)2} = p^{(n)2} = \frac{1}{R^2}$, where R is the radius of the compactified dimension. The zero modes correspond to a massless Standard Model graviton, photon and Goldstone boson. In non-zero modes the gauge graviton field gains a mass by absorbing the two degrees of freedom from the vector Goldstone and scalar Goldstone boson fields to yield a pure spin 2 particle with five degrees of freedom and charges $e^{(n)}$ and masses $m^{(n)}$

$$e^{(n)} = n\sqrt{2}\kappa m^{(0)}, m^{(n)} = |n|m^{(0)} \quad (8.1.2)$$

where $\kappa = 8\pi G$. If the fundamental unit of charge is taken to be that of an electron, this means the masses are of the scale Planck mass 10^{19} GeV in the original theory. [7]

Difficulties with the Kaluza-Klein model including the origin of fermions and how to solve the Hierachy Problem led to additional theories using extra dimensions, including large extra dimensions (ADD model) and warped extra dimensions (Randall-Sundrum model), which introduce modifications to the bulk geometry and zero mode mass scales of $O(\text{TeV})$.

8.1.1 Bulk Fermions in Warped Extra Dimensions

Warped extra dimensions or the Randall-Sundrum scenario (RS1) is a proposed solution to the Hierachy Problem in which the graviton is contained on the ‘‘Planckbrane’’ due to a high warped fifth-dimension with a probability function that drops rapidly towards the ‘‘TeVbrane’’ containing the Higgs sector by the inclusion of a factor of $e^{-k|\theta|R}$. This change in energy scale by 16 orders of magnitude is devised to explain gravity’s weakness in the Tevbrane. The flavour problem of an $O(10^3)$ TeV energy scale arising from FCNC’s can be solved by additionally propogating Standard Model gauge and fermion fields into the bulk. In five dimensions fermions are vector-like, and can be given a 5D Dirac mass term parameterised by $m_\Psi = c \cdot k \text{sgn}(y)$, where y is the 5th coordinate. The value of c determines whether the zero mode is localised towards the Planckbrane ($c > \frac{1}{2}$) or Tevbrane ($c < \frac{1}{2}$). By choice of this parameter, light fermion FCNC’s can be straightforwardly suppressed in the theory, as their zero modes are localised to the Planckbrane if $c > \frac{1}{2}$. For the top quark, however, the requirement of setting up a $O(1)$ Yukawa coupling to the Higgs on the Tevbrane necessitates a choice of $c < \frac{1}{2}$. The localisation of a left-handed top quark near the Tevbrane will result in FCNC’s involving b_L through the gauge Kaluza-Klein modes, similar to graviton exchange. [9]

Flavour-violating couplings of zero-mode fermions to gauge Kaluza-Klein n -modes result during unitary transformation D_L from weak to mass eigenstate basis for left-handed down quarks:

$$D_L^\dagger \text{diag} \left[g^{(n)}(c_{Ld}), g^{(n)}(c_{Ls}), g^{(n)}(c_{Lb}) \right] D_L \quad (8.1.3)$$

Coupling between b to Kaluza-Klein gluons in pure penguin processes $b \rightarrow s\bar{s}s$ and $b \rightarrow s\bar{d}d$ such as $B_d \rightarrow \phi K_s^0$, $B_d \rightarrow \eta' K_s^0$ and $B_d \rightarrow \pi^0 K_S^0$ can make significant contributions due to Standard Model tree level amplitude suppression. In the case of $b \rightarrow s$, the cooefficient from $(\bar{b}_L \gamma^\mu s_L)^2$ is given by

$$[(D_L)_{bs}]^2 \sum_n g^{(n)2} / M_G^{(n)2} \quad (8.1.4)$$

where M_G is the Kaluza-Klein gluon mass of $O(\text{TeV})$. While large uncertainties are expected when calculating the branching ratios for these modes, they are expected to largely cancel in CP asymmetries. Observable differences from the Standard Model for $\sin(2\phi_1)$ can be made and plotted for various decay amplitude phases ω in d. Similar effects occur in the pure penguin decays, as well as in B_s and B_d oscillations in mixing. [8]

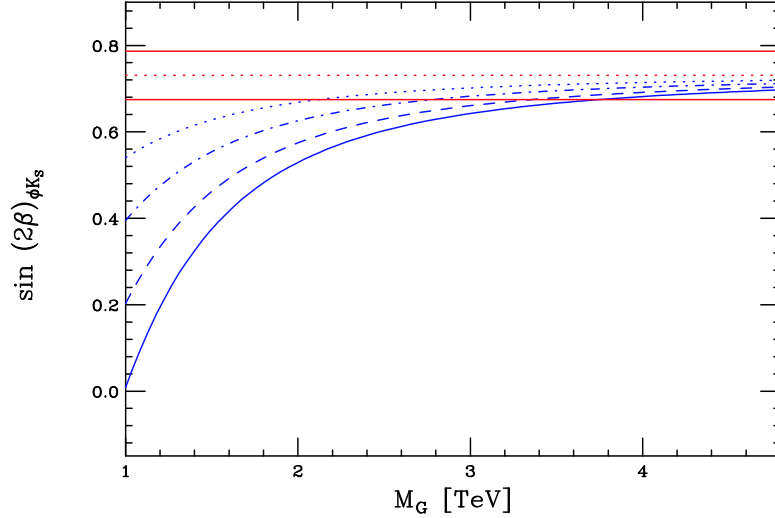


Figure 8.1.1: $\sin(2\phi_1)_{\phi K_S}$ distribution in the KK gluon mass for decay amplitude phases (bottom to top) $\omega = \frac{\pi}{3}, \frac{\pi}{4}, \frac{\pi}{6}, \frac{\pi}{10}$. The red horizontal band is the world average value for the SM $b \rightarrow c\bar{c}s$ tree level process $B_d \rightarrow J/\psi K_S^0$, $\sin(2\phi_1)_{\psi K_S^0}$

In b_L to Z^0 coupling, adjusted values for allowed shifts in $g_Z^{b_L}$ of $O(1\%)$ from precision electroweak measurements result in modifications to $b \rightarrow s\ell^+\ell^-$ decays through

$$b_L s_L Z \sim 1\% V_{ts} \quad (8.1.5)$$

relative to to the standard coupling of d_L to Z^0 . This effect of same order as the Standard Model has a $\sim 15\%$ theoretical error and should be observable at high-luminosity colliders. [9]

8.1.2 Kaluza-Klein Graviton Exchange

The flavour structure of tower graviton interaction with Standard Model fields can be illuminated in rare $b \rightarrow s\ell^+\ell^-$ decays. At low-energies, the exchange can be described by an operator common to large and warped extra dimension models though

$$O_{grav} = \frac{1}{M_H^4} X T_{\mu\nu} T^{\mu\nu} \quad (8.1.6)$$

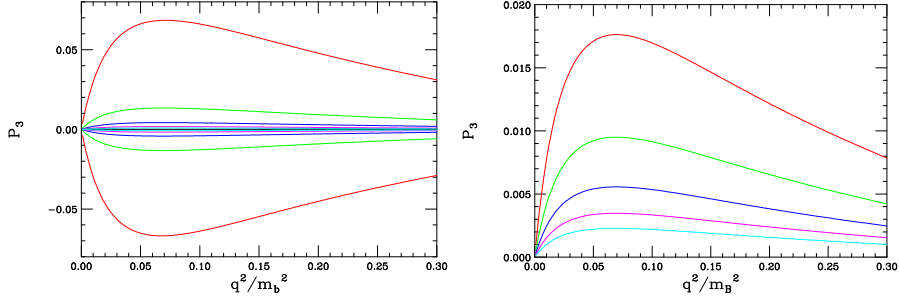


Figure 8.1.2: $\langle P_3 \rangle$ as a function of scaled momentum transfer s for different graviton scenarios; $M_H = 1, 1.5, 2 \dots$ TeV for the ADD model (left) and first-mode graviton masses 600 (red), 700, ... GeV for the Randall-Sundrum (right) models

where M_H is the zero mode mass scale of $O(\text{TeV})$, X a general coupling matrix and $T_{\mu\nu}$ are the stress-energy tensors of the Standard Model fields. The $T_{\mu\nu}$ terms are modified by the graviton vertices for $b\bar{s}$ and $\ell^+\ell^-$ respectively, resulting in a modified differential decay distribution. A unique feature that can be used distinguish graviton exchange from other new physics processes is a $\cos^3\theta$ dependence on the lepton pair decay angle, resulting from a spin 2 exchange in the s -channel. [8] This can be represented in terms of the third Legendre polynomial P_3 , in the quantity

$$\langle P_3(s) \rangle = \frac{\int \frac{d^2\Gamma}{dsdz} P_3(z) dz}{\frac{d\Gamma}{ds}} \quad (8.1.7)$$

where $z = \cos(\theta)$ and s is the scaled momentum transfer $s = q^2/m_b^2$.

Statistics of the order $50 \sim 100 \text{ ab}^{-1}$ will be necessary to make such an observation at Belle II. [8]

Bibliography

- [1] “Letter of Intent for KEK Super B Factory: Part I Physics” (April 2004); <http://superb.kek.jp/documents/loi/loi.html>
- [2] “Letter of Intent for KEK Super B Factory: Part II Dectector” (April 2004); <http://superb.kek.jp/documents/loi/loi.html>
- [3] “Letter of Intent for KEK Super B Factory: Part III Accelerator” (April 2004); <http://superb.kek.jp/documents/loi/loi.html>
- [4] Oide, K., “KEKB B-Factory, The Luminosity Frontier” (June 2009); Progress of Theoretical Physics 122-1
- [5] T.Browder, M.Ciuchini, T.Gershon, M.Hazumi, T.Hurth, Y.Okada, A.Stocchi, “On the Physics Case of a Super Flavour Factory” (October 2007); arXiv:0710.3799[hep-ph]
- [6] Hewett, J., Spiropulu, M, “Particle Physics Probes Of Extra Spacetime Dimensions” (May 2002); arXiv:hep-ph/0205106v1
- [7] Duff, M. J., “Kaluza-Klein Theory in Perspective” (October 1994); arXiv:hep-th/9410046
- [8] Hewett, J., Hitlin, G. et al, “The Discovery Potential of a Super *B* Factory” (December 2004); <http://www.slac.stanford.edu/cgi-wrap/pubpage?slac-r-709>
- [9] Agashe, Kaustubh, Perez, Gilad, & Soni, Amarjit. (2004). B-factory signals for a warped extra dimension. Lawrence Berkeley National Laboratory: Lawrence Berkeley National Laboratory. Retrieved from: <http://escholarship.org/uc/item/2j35v03b>
- [10] Wille, K., *The Physics of Particle Accelerators*, Oxford 2000, chapter 3
- [11] Wiedemann, H., *Particle Accelerator Physics Third Edition*, Springer 2007, chapter 5
- [12] Milardi, C., “DAΦNE Setup and Operation with the Crab-Waist Collision Scheme”, EPAC08 p2599-2601

- [13] Chao, A. et al, *Handbook of Accelerator Physics and Engineering*, World Scientific 1999, p233
- [14] Lockman, W. S.. et al, “Geant-4 Based Simulation Study of PEP-II Beam Backgrounds in the BaBar Detector at the SLAC B-Factory” (2005); <http://accelconf.web.cern.ch/Accelconf/p05/PAPERS/WPAE056.PDF>
- [15] Sad Home Page; <http://acc-physics.kek.jp/SAD/>
- [16] Tanabe, K., “Simulation Study of Linear Collider Beam Delivery System” (talk), ISG9; <http://hep.phys.s.u-tokyo.ac.jp/~tanabe/LC/files/ISG9BDSG4.pdf>
- [17] Geant4 Home Page; <http://geant4.web.cern.ch/geant4/>
- [18] Jadach, S., et al, “Upgrade of the Monte Carlo program BHLUMI for Bhabha scattering at low angles to version 4.04” (June 1996); <http://jadach.web.cern.ch/jadach/th-96-158/th-96-158.html>